Mon. Not. R. Astron. Soc. **350,** 1511–1535 (2004) doi:10.1111/j.1365-2966.2004.07742.x

The GEMS project: X-ray analysis and statistical properties of the group sample

John P. F. Osmond★ and Trevor J. Ponman
School of Physics and Astronomy, The University of Birmingham, Edgbaston, Birmingham B15 2TT

Accepted 2004 February 17. Received 2004 February 6; in original form 2003 October 2

ABSTRACT

The Group Evolution Multiwavelength Study (GEMS) involves a multiwavelength study of a sample of 60 galaxy groups, chosen to span a wide range of group properties. Substantial *ROSAT* Position Sensitive Proportional Counter (PSPC) observations, available for all of these groups, are used to characterize the state of the intergalactic medium in each. We present the results of a uniform analysis of these *ROSAT* data and a statistical investigation of the relationship between X-ray and optical properties across the sample. Our analysis improves in several respects on previous work: (i) we distinguish between systems in which the hot gas is a group-scale medium and those in which it appears to be just a hot halo associated with a central galaxy; (ii) we extrapolate X-ray luminosities to a fixed overdensity radius (r_{500}) using fitted surface brightness models, in order to avoid biases arising from the fact that cooler systems are detectable to smaller radii, and (iii) optical properties have been rederived in a uniform manner from the NASA Extragalactic Database, rather than relying on the data in the disparate collection of group catalogues from which our systems are drawn.

The steepening of the L_{X}–T_{X} relation in the group regime reported previously is not seen in our sample, which fits well on to the cluster trend, albeit with large non-statistical scatter. A number of biases affect the fitting of regression lines under these circumstances, and until the impact of these has been thoroughly investigated it seems best to regard the slope of the group $L_{\mathrm{X}}-T_{\mathrm{X}}$ relation as being poorly determined. A significant problem in comparing the properties of groups and clusters is the derivation of system radii, to allow different systems to be compared within regions having the same overdensity. We find evidence that group velocity dispersion (σ_{v}) provides a very unreliable measure of system mass (and hence radius), with a number of groups having remarkably low values of σ_{v}, given that they appear from their X-ray properties to be collapsed systems. We confirm that the surface brightness profiles of groups are significantly flatter than those of clusters – the maximum value of the β_{fit} parameter for our sample is 0.58, lower than the typical value of 0.67 seen in clusters – however, we find no significant tendency within our sample for cooler groups to show flatter profiles. This result is inconsistent with simple universal pre-heating models. The morphology of the galaxies in the GEMS groups is correlated to their X-ray properties in a number of ways: we confirm the very strong relationship between X-ray emission and a dominant early-type central galaxy, which has been noted since the early X-ray studies of groups, and also find that spiral fraction is correlated with the temperature of the hot gas and hence the depth of the gravitational potential. A class of spiral-rich groups with little or no X-ray emission probably corresponds to groups that have not yet fully collapsed.

Key words: galaxies: clusters: general – galaxies: evolution – galaxies: formation – galaxies: general – intergalactic medium – X-rays: galaxies: clusters.

1 INTRODUCTION

The principle that we are nowhere special, which is fundamental to cosmology, also applies to galaxies. The majority of galaxies are,

★E-mail: jpfo@star.sr.bham.ac.uk

like our own, located within bound systems, mostly containing just a handful of bright galaxies (Tully 1987). These are characterized as galaxy groups, which are distinguished rather arbitrarily from richer and rarer galaxy clusters. These systems are evolving, as they turn round from the Hubble expansion, virialize and grow through mergers and accretion. This dynamical evolution modifies the environment of their constituent galaxies and can in turn have profound effects on the evolution of the galaxies themselves. On the other hand, energetic galaxy winds can have a substantial impact on the surrounding intergalactic medium (IGM) within groups and clusters (e.g Ponman, Cannon & Navarro 1999), so that there is a two-way interaction between the structure of galaxies and galaxy systems. The picture that emerges is that galaxies and the systems in which most of them are located co-evolve and a full understanding of the evolution of either galaxies or galaxy clusters must take into account the two-way interactions that couple the development of both.

Galaxy groups have received far less attention from astronomers than either galaxies or galaxy clusters, and their properties are clearly very diverse, in terms of structure, dynamics and the types of galaxies they contain (Hickson 1997; Zabludoff & Mulchaey 1998; Mulchaey 2000). Any meaningful study of the relationship between groups and galaxies needs to acknowledge this fact. Therefore, we have commenced a study of the properties of a substantial sample of 60 galaxy groups and the galaxies they contain, with a view to clarifying the different stages of group evolution and the ways in which this is related to galaxy properties. This Group Evolution Multiwavelength Study (GEMS) project involves optical photometry and spectroscopy to study the galaxies, radio observations to explore the H I content of galaxies and to look for cool intergalactic gas, and X-ray studies to probe the hot gas that dominates the baryonic content of at least some galaxy groups and also provides a valuable indicator that a group is truly a dense system in three dimensions.

Given the value of X-ray data, all groups in our sample have been selected to have high-quality *ROSAT* observations available: though we have not selected only groups that are detected in the X-ray. The present paper describes the analysis of these *ROSAT* Position Sensitive Proportional Counter (PSPC) data and the properties derived from them, and combines these with other properties of these systems and their galaxies drawn from the literature and, in particular, from the NASA–IPAC Extragalactic Database (NED). There have been a number of previous studies of samples of galaxy groups based primarily on pointed *ROSAT* observations (e.g. Pildis, Bregman & Evrard 1995; Mulchaey et al. 1996; Ponman et al. 1996; Mulchaey & Zabludoff 1998; Helsdon & Ponman 2000a,b; Mulchaey et al. 2003, the latter hereafter referred to as MDMB).

The present work improves on these in a number of respects:

(i) it is one of the largest samples for which the X-ray data have been analysed in a uniform manner;

(ii) it includes systems with low X-ray luminosity and some that are entirely undetected in the X-ray;

(iii) systems showing intergalactic X-ray emission have been distinguished from those in which the X-ray emitting gas appears to constitute only hot halo gas associated with the central galaxy;

(iv) galaxy membership and internal velocity dispersion of the groups have been rederived in a consistent way, usingthe NED data and a sigma-clipping approach, within a projected overdensity radius;

(v) fitted models have been used to extrapolate X-ray luminosity to a fixed overdensity radius, to compensate for systematic trends with temperature in the radial extent to which X-ray data are available.

The only other studies that share some (but not all) of these features are those of Helsdon & Ponman (2000a,b) and MDMB, with which we make a number of comparisons below.

Throughout this paper we use $H_0 = 70$ km s^{-1} Mpc^{-1}, and all errors correspond to 1σ.

2 THE SAMPLE

We have sought to assemble the largest sample of galaxy groups for which an X-ray analysis can be performed. Therefore, we have compiled a list of 4320 groups from 10 optical catalogues (Hickson 1982; Huchra & Geller 1982; Geller & Huchra 1983; Fouque et al. 1992; Garcia 1993; Nolthenius 1993; Barton et al. 1996; Ramella, Pisani & Geller 1997; Giudice 1999; White et al. 1999) and compared it to the *ROSAT* PSPC observation log. Groups with a recessional velocity in the range $1000 < v < 3000$ km s^{-1} were then selected from this list if there was a PSPC pointing with $t > 10\,000$ s, within 20 arcmin of the group position. This was to ensure the availability of good quality *ROSAT* data and that the system was neither so close as to overfill the PSPC field of view nor so distant as to make an X-ray detection unlikely.

Duplicate entries resulting from the overlap between catalogues were removed, along with seven groups in or around the Hydra and Virgo clusters. One further system, NGC 7552 (drawn from Huchra & Geller 1982), was excluded after a calculation of the optical membership described in Section 3 revealed that, although the catalogued group position adhered to all of the above criteria, the group galaxies are all located at radii >20 arcmin from the *ROSAT* PSPC pointing, so that none of them actually lie within the mirror shell support ring of the PSPC.

To the resulting sample of 45 selected groups, we added a further 13 that had previously been studied with the PSPC by Helsdon & Ponman (2000a), who in turn assembled their sample from those of Nolthenius (1993), Ledlow et al. (1996); Mulchaey & Zabludoff (1998), and two additional Hickson compact groups (HCG 4 and 40) for which we had collected useful optical data. The resulting ensemble of groups is clearly not a true statistical sample, but is chosen to represent a wide range of group properties.

Details of the full sample of 60 groups can be found in Table 1, where the names given are taken from the optical catalogues that have been used and generally (apart from the Hickson compact groups) correspond to the name of a prominent galaxy within the group. The group positions given in Table 1, were defined in the following way: (i) where X-ray emission is present (i.e. most cases), the position is that of the galaxy most centrally located within this emission; (ii) where no X-rays are detected, the catalogued group position was used. Note that, following these rules, group positions do not always correspond to the location of the galaxy whose name appears in the first column of Table 1.

We have further segregated our sample into three subsamples according to the presence and nature of their X-ray emission, because it is important to distinguish between emission that is genuinely intergalactic and that which appears to be associated with the halo of an individual galaxy. It has been shown that the emission from X-ray bright groups is typically characterized by a two-component surface brightness profile (Mulchaey & Zabludoff 1998), where the extended component corresponds to the group emission and the central component to either the central galaxy or a bright group core. Therefore, the presence of two such components confirms that a group contains intergalactic hot gas. Unfortunately, poor statistics can often make fitting a two-component model difficult, even if the distribution is truly two-component, and in such cases a

Table 1. The sample listed in order of right ascension (Section 2). RA and Dec. are defined as discussed in the text. v, σ_v and N_{gal} are taken from the respective catalogues and are rederived in Table 2 for use in the present work. Groups where the catalogue is marked with *have been included from the Helsdon & Ponman (2000a) sample and parameters were taken from that paper. Velocity dispersions of Hickson compact groups are taken from Ponman et al. (1996).

Group name	RA (J2000)	Dec. (J2000)	v (km s^{-1})	σ_v (km s^{-1})	N_{gal}	Catalogue
HCG 4	00 34 13.8	−21 26 21	8394	n/a	5	Hickson (1982)
NGC 315	00 57 48.9	+30 21 09	4920	122	4	*Nolthenius (1993)
NGC 383	01 07 24.9	+32 24 45	5190	466	29	*Ledlow et al. (1996)
NGC 524	01 24 47.8	+09 32 19	2632	167	9	Garcia (1993)
NGC 533	01 25 31.3	+01 45 33	5430	464	36	*Mulchaey & Zabludoff (1998)
HCG 10	01 25 40.4	+34 42 48	4827	240	4	Hickson (1982)
NGC 720	01 53 00.4	−13 44 18	1760	162	4	Garcia (1993)
NGC 741	01 56 21.0	+05 37 44	5370	432	41	*Mulchaey & Zabludoff (1998)
HCG 15	02 07 37.5	+02 10 50	6835	457	6	Hickson (1982)
HCG 16	02 09 24.7	−10 08 11	3957	135	4	Hickson (1982)
NGC 1052	02 41 04.8	−08 15 21	1477	93	14	Garcia (1993)
HCG 22	03 03 31.0	−15 41 10	2700	13	5	Hickson (1982)
NGC 1332	03 26 17.1	−21 20 05	1499	n/a	n	Barton et al. (1996)
NGC 1407	03 40 11.8	−18 34 48	1695	151	8	Garcia (1993)
NGC 1566	04 20 00.6	−54 56 17	1292	99	6	Garcia (1993)
NGC 1587	04 30 39.9	+00 39 43	3660	106	4	*Nolthenius (1993)
NGC 1808	05 07 42.3	−37 30 46	1141	213	6	Giudice (1999)
NGC 2563	08 20 35.7	+21 04 04	4890	336	29	*Mulchaey & Zabludoff (1998)
HCG 40	09 38 54.5	−04 51 07	6685	162	6	Hickson (1982)
HCG 42	10 00 14.2	−19 38 03	3840	240	4	Hickson (1982)
NGC 3227	10 23 30.6	+19 51 54	1407	118	4	Ramella et al. (1997)
HCG 48	10 37 49.5	−27 07 18	2818	355	4	Hickson (1982)
NGC 3396	10 49 55.2	+32 59 27	1578	96	6	Garcia (1993)
NGC 3557	11 09 57.4	−37 32 17	2635	377	11	Garcia (1993)
NGC 3607	11 16 54.7	+18 03 06	1232	245	10	Ramella et al. (1997)
NGC 3640	11 21 06.9	+03 14 06	1260	178	6	Garcia (1993)
NGC 3665	11 24 43.4	+38 45 44	2076	65	5	Garcia (1993)
NGC 3783	11 39 01.8	−37 44 19	2819	169	4	Giudice (1999)
HCG 58	11 42 23.7	+10 15 51	6206	178	5	Hickson (1982)
NGC 3923	11 51 02.1	−28 48 23	1376	103	5	Garcia (1993)
NGC 4065	12 04 06.2	+20 14 06	7050	495	9	*Ledlow et al. (1996)
NGC 4073	12 04 27.0	+01 53 48	6120	607	22	*Ledlow et al. (1996)
NGC 4151	12 10 32.6	+39 24 21	1358	95	3	Ramella et al. (1997)
NGC 4193	12 13 53.6	+13 10 22	2695	168	4	Nolthenius (1993)
NGC 4261	12 19 23.2	+05 49 31	2355	120	18	Garcia (1993)
NGC 4325	12 23 06.7	+10 37 16	7560	256	18	*Mulchaey & Zabludoff (1998)
NGC 4589	12 21 45.0	+75 18 43	2027	147	11	Garcia (1993)
NGC 4565	12 36 20.8	+25 59 16	1245	62	3	Giudice (1999)
NGC 4636	12 42 50.4	+02 41 24	1696	475	12	Nolthenius (1993)
NGC 4697	12 48 35.7	−05 48 03	1363	241	7	Giudice (1999)
NGC 4725	12 50 26.6	+25 30 06	1495	17	4	Ramella et al. (1997)
HCG 62	12 53 05.8	−09 12 16	4380	324	4	Hickson (1982)
NGC 5044	13 15 24.0	−16 23 06	2460	129	9	Garcia (1993)
NGC 5129	13 24 10.0	+13 58 36	6960	294	33	*Mulchaey & Zabludoff (1998)
NGC 5171	13 29 21.6	+11 44 07	6960	424	8	*Ledlow et al. (1996)
HCG 67	13 49 11.4	−07 13 28	7345	240	4	Hickson (1982)
NGC 5322	13 49 15.5	+60 11 28	2106	176	8	Garcia (1993)
HCG 68	13 53 26.7	+40 16 59	2400	170	5	Hickson (1982)
NGC 5689	14 34 52.0	+48 39 36	2226	n/a	3	White (1999)
NGC 5846	15 06 29.2	+01 36 21	1890	368	20	*Mulchaey & Zabludoff (1998)
NGC 5907	15 15 53.9	+56 19 46	1055	56	4	Geller & Huchra (1983)
NGC 5930	15 26 07.9	+41 40 34	2906	70	3	Ramella et al. (1997)
NGC 6338	17 15 22.9	+57 24 40	8490	589	7	*Ledlow et al. (1996)
NGC 6574	18 12 00.7	+14 02 44	2435	34	4	Garcia (1993)
NGC 7144	21 52 42.9	−48 15 16	1855	105	5	Garcia (1993)
HCG 90	22 02 08.4	−31 59 30	2640	110	4	Hickson (1982)
HCG 92	22 35 58.4	+33 57 57	6446	447	5	Hickson (1982)
IC 1459	22 57 10.6	−36 27 44	1707	144	5	Garcia (1993)
NGC 7714	23 36 14.1	+02 09 19	2908	152	n/a	Fouque et al. (1992)
HCG 97	23 47 22.9	−02 18 02	6535	407	5	Hickson (1982)

one-component model may be all that is available. Hence some other criterion is required, which can discriminate between group-scale and galaxy halo emission, even in the case of poor quality data. Two simple criteria were investigated: the detectable extent of group emission ($r_{\rm ext}$, Section 4.1) and the ratio of X-ray luminosity to the luminosity of the central brightest group galaxy (BGG; $L_{\rm X}/L_{\rm BGG}$). The former was found to give more satisfactory results, in that a simple threshold in $r_{\rm ext}$ of 60 kpc was found to result in the classification all two-component systems as X-ray groups. Therefore, we assumed that any systems with one-component fits, which had emission more extensive than 60 kpc, also possessed intergalactic gas, but that poor quality data did not permit a two-component fit.

The implication of our extension threshold is that individual galaxies should not have X-ray haloes extending to more than 60 kpc in radius. To check this, it would be useful to compare our threshold value of $r_{\rm ext}$ with the radii derived from a sample of isolated early-type galaxies (late-type galaxies have much less extended hot gas haloes). Unfortunately, isolated early-type galaxies are rare and very few have been studied with X-ray instruments. O'Sullivan, Ponman & Collins (2003) studied *ROSAT* data from a sample of 39 early-type galaxies, of which eight were neither BGGs, nor brightest cluster galaxies. The X-ray radii of these galaxies ranged from ~3 to 9 kpc: much smaller than our threshold. A recent study, by O'Sullivan & Ponman (2004), of a rather X-ray bright isolated elliptical galaxy, NGC 4555, detected emission extending to just 60 kpc. Hence, this would have (just) been correctly classified by our extension criterion.

As a further check, we also examined $L_{\rm X}/L_{\rm BGG}$ for all groups and found one case in which we felt that our extension criterion had failed. In HCG 22, the X-ray emission is centred on a rather faint elliptical ($L_{\rm B} = 10^{9.29}\ {\rm L}_\odot$) and the BGG lies outside the main X-ray emitting region. Using this dimmer central galaxy to calculate $L_{\rm X}/L_{\rm B}$ results in a value of $10^{31.39}$ erg s^{-1} L$_\odot^{-1}$, which is significantly higher than the maximum value for any other galaxy halo system ($L_{\rm X}/L_{\rm BGG} = 10^{30.75}$ erg s^{-1} L$_\odot^{-1}$). Therefore, we have altered the classification of this system from galaxy halo to group emission, to reflect its high value of $L_{\rm X}$, relative to its optically dim central galaxies.

Finally, groups with an X-ray flux ($L_{\rm X}$, Section 4.2) less than 3σ above the background level have been classed as X-ray undetected groups. Therefore, we have the following three subsamples:

(i) G-sample: 37 groups (36 with $r_{\rm ext} > 60$ kpc and HCG 22)
(ii) H-sample: 15 groups with $r_{\rm ext} \leqslant 60$ kpc
(iii) U-sample: 8 groups with $L_{\rm X} < {\rm bg} + 3\sigma({\rm bg})$

Selection effects in our sample originate from the requirement to have *ROSAT* archive data available, the velocity cut we have used and the sample of Helsdon & Ponman (2000a) from which a large fraction of our groups have been taken. It is not clear what biasing is inherent in the *ROSAT* pointing agenda. Some of our targets were observed serendipitously by *ROSAT*, which reduces any bias involved, but most were the subject of direct pointed observations. Our sample should therefore be viewed as diverse (and in particular it is not restricted to X-ray bright systems) rather than statistically representative. Details of the 60 groups in our full sample are given in Table 1.

3 OPTICAL PROPERTIES

Our groups have been assembled from a large number of catalogues and, in order to reduce the inhomogeneity in our optical data, we have rederived their galaxy membership in a uniform manner. Group galaxies were selected from the NED using the algorithm described below and optical properties such as total B-band luminosity, morphological type, velocity and position were extracted. However, there will remain a degree of inhomogeneity in the NED data, as a result of the range of sources from which the NED data have been compiled. We discuss some checks on the effects of this heterogeneity, later in this section.

For each group we have searchedthe NED for galaxies within a projected radius r_{500} of the group position, defined above, and in a velocity range of $v \pm 3\sigma_{\rm v}$. Values of r_{500} were calculated from temperature ($T_{\rm X}$, Section 4.2) using a relation derived from simulations by Evrard, Metzler & Navarro (1996),

$$r_{500}(T_{\rm X}) = \frac{124}{H_0}\sqrt{\frac{T_{\rm X}}{10\,{\rm keV}}}\,{\rm Mpc}, \qquad (1)$$

where $T_{\rm X}$ is the temperature in keV and H_0 is the Hubble constant in km s^{-1} Mpc^{-1}. Where no value of $T_{\rm X}$ was available, a relation between r_{500} and $L_{\rm B}$ was derived using equation (1) and a regression fit in the $L_{\rm B} - T_{\rm X}$ plane for the systems with group-scale emission (Section 4.3),

$$r_{500}(L_{\rm B}) = \frac{124}{H_0}\sqrt{\frac{1}{10}\left(\frac{L_{\rm B}}{10^{11.33}}\right)^{1/1.28}}\,{\rm Mpc}. \qquad (2)$$

A value of r_{500} can also be estimated from galaxy velocity dispersion, using the virial theorem. Assuming energy equipartition between gas and galaxies (i.e. $\beta_{\rm spec} = 1$, see Section 4.2), equation (1) can be rewritten in terms of $\sigma_{\rm v}$,

$$r_{500}(\sigma_{\rm v}) = \frac{0.096\sigma_{\rm v}}{H_0}\,{\rm Mpc}, \qquad (3)$$

where $\sigma_{\rm v}$ is the velocity dispersion in km s^{-1}. However we find evidence that this method is unreliable at low values of $\sigma_{\rm v}$, as discussed in Section 6.

Starting values of v and $\sigma_{\rm v}$ were taken from the respective catalogues. It has been shown that a virialized group should have $\sigma_{\rm v} \gtrsim 100$ km s^{-1} (Mamon 1994) and, as such, we have constrained our starting value of $\sigma_{\rm v}$ to be no less than this. In cases where no value of velocity dispersion was available from the source catalogue, we have used 200 km s^{-1}.

Optical data resulting from the galaxy extraction were used to recalculate v and $\sigma_{\rm v}$, where

$$\sigma_{\rm v} = \sqrt{\frac{\sum(v-\bar{v})^2}{N-\frac{3}{2}}} \pm \frac{\sigma_{\rm v}}{\sqrt{2\left(N-\frac{3}{2}\right)}}\,{\rm km\,s^{-1}} \qquad (4)$$

and the updated values used to redefine our search criteria. The denominator includes a correction for the effects of biasing in systems with a small number of galaxies (Helsdon & Ponman, in preparation). The selection and recalculation were then repeated until the values of v and $\sigma_{\rm v}$ became stable. If the final number of galaxies within a group was less than three, then the membership calculation was repeated with the starting value of $\sigma_{\rm v}$ set to 200 km s^{-1}. Distances (D) were calculated from velocities after correcting for infall into Virgo and the Great Attractor.

For two of our systems it was necessary to adjust the membership calculation in order to reduce contamination from nearby clusters. NGC 4261 is in the vicinity of two clusters (WBL 392 and 397) and to prevent the $\sigma_{\rm v}$ from increasing to include cluster galaxies, we have used only one iteration of the membership calculation. HCG 48 is falling into the cluster Abell 1060, and to reduce contamination we have used a group radius equivalent to the distance away of the minimum in the galaxy density distribution between the centre of the two systems.

We improve the completeness of our sample by applying a luminosity cut to the optical selection. The value of luminosity was chosen so as to include 90 per cent of the *B*-band luminosity of the galaxy population, as described by a Schechter function of the form

$$\phi(L)\,\mathrm{d}L = \phi_\star \left(\frac{L}{L_\star}\right)^{\alpha} \exp\left(-\frac{L}{L_\star}\right)\frac{\mathrm{d}L}{L_\star}, \qquad (5)$$

where L is the galaxy luminosity and $\phi(L)\,\mathrm{d}L$ is the number of galaxies with a luminosity between L and $L + \mathrm{d}L$ per Mpc^3. Free parameters are the slope at the faint end (α), the characteristic Schechter luminosity ($L_\star$) and the normalization ($\phi_\star$). We have taken values of α and $L_\star$ from Zabludoff & Mulchaey (2000) and applied a correction of $B - R = 1.57$ to convert from *R*-band to *B*-band magnitudes (Fukugita, Shimasaku & Ichikawa 1995) giving $\alpha = -1.3$, $L_\star = 1.60 \times 10^{10}\,\mathrm{L}_\odot$ and a minimum luminosity of $L_{\mathrm{cut}} = 5.28 \times 10^8\,\mathrm{L}_\odot$ (corresponding to $M_\mathrm{B} = -16.32$). We investigate the completeness obtained by applying this cut in our comparison with Miles et al. (2004) below. The assumed value of $B - R$ is appropriate for early-type galaxies and in the case of late types it will typically result in a luminosity cut that is too low by approximately 0.5 mag. However, no correction has been applied for the effects of extinction on our galaxy magnitudes and for typical spirals this amounts to $\sim$0.5 mag in the *B*-band. Hence, the two effects approximately cancel and our galaxy membership cut should be reasonably accurate.

We have applied this cut following the membership calculation and, as such, it does not affect the calculated values of v and σ_v, which are based on the full sample of galaxies associated with each group. Data surviving the cut were used to calculate total optical luminosity L_B, corrected for the effect of the magnitude cut, spiral fraction by number, f_{sp}, and mean galaxy density, $\bar{\rho}_{\mathrm{gal}}$, assuming a spherical volume of radius r_{500}. The brightest galaxy within $0.25r_{500}$ of the the group position was designated as the BGG and its luminosity (L_{BGG}) was divided by the luminosity of the second brightest galaxy to define the dominance of the BGG (L_{12}). The results of the membership calculation are shown in Table 2. The number of galaxies (N_{gal}) is quoted both before and after the luminosity cut. Systems with $N_{\mathrm{gal}} < 4$ before the luminosity cut have been excluded from the statistical analysis, on the grounds that (i) many of the optical properties of interest to us are poorly defined for these systems, and (ii) such very poor systems are quite likely to be line-of-sight projections, rather than genuinely overdense in three dimensions (Frederic 1995). This richness cut excludes six groups, two of which have group-scale X-ray emission, but with statistical quality too poor to derive an X-ray temperature. These six systems are included in the main data tables, but are flagged with daggers in Tables 2, 3 and 4.

Hence, our sample for statistical analysis in the present paper consists of 54 GEMS groups, which are divided into three subsets according to their X-ray properties. We refer to these below as the G-sample (35 systems) that has group-scale emission, the H-sample (13 systems) with galaxy halo emission and the U-sample (6 systems) that are undetected in X-rays.

As discussed above, the optical data drawn from the NED are inevitably inhomogeneous. To investigate the effects of this on our optical luminosities, we have compared our optical results to those of Miles et al. (2004), who obtained *B*-band photometry for a subset of 25 of the GEMS groups. Fig. 1 shows a comparison between our galaxy luminosities and those of Miles et al. (2004) for each galaxy that appears in both samples. Assuming the Miles et al. (2004) data to be accurate, we find that our luminosities appear to be biased high (by $\approx$20 per cent) for the brightest galaxies and low (by $\approx$50 per cent) for faint ones. However, agreement for $L_\mathrm{B} \sim L_\star = 10.20$, where most of the total optical luminosity resides, is good, so that our estimates of total optical luminosity for groups should be substantially unbiased.

We also derive a luminosity function from our data using galaxies that are associated with groups in the Miles et al. (2004) subsample and are situated within their extraction radii of $r = 0.3\,r_{500}$. Fig. 2 shows a comparison of this luminosity function with that derived by Miles et al. (2004). We find 81 galaxies above our luminosity cut of $M_\mathrm{B} = -16.32$ compared to the 90 found by Miles et al. (2004). Because it is clear from Fig. 2 that the Miles et al. (2004) luminosity function is complete to a magnitude much fainter than our cut, we conclude that our sample is approximately 90 per cent (81/90) complete, down to our cut.

A further check on the completeness of our sample close to the cut is obtained by comparing the total light in galaxies above two different cuts. Using equation (5) we calculate the luminosity above which 50 per cent of the optical light should lie, to be 1.34×10^{43} erg s^{-1}($M_\mathrm{B} = -20.55$). If our sample were complete to the 90 per cent cut then we would expect the ratio of total light above the two cuts to be $\sum L_\mathrm{B}(90\,\text{per cent})/\sum L_\mathrm{B}(50\,\text{per cent}) = 1.8$. In practice, this ratio is found to be 1.9 for our data, suggesting that our completeness is still very high down to the 90 per cent cut, under the assumption that our galaxy luminosity function is well represented by the adopted Schechter function.

4 X-RAY DATA ANALYSIS

ROSAT PSPC data sets were prepared for analysis by first eliminating sources of contamination such as particle emission and solar X-ray emission scattered from the atmosphere of the Earth. Detectors aboard the spacecraft identify and exclude over 99 per cent of these events and record them in a master veto file. Times for which this master veto rate exceeded 170 count s^{-1} were considered significantly contaminated and excluded from our analysis. Further contamination from reflected solar X-rays can be identified by an increase in the total X-ray event rate. To remove this contamination we have excluded all times for which the total event rate exceeded the mean by greater than 2σ. The remaining counts were binned into a three-dimensional x, y, energy data cube. Images were created by projecting the data cube along its energy axis and smoothed images were generated by convolving with a two-dimensional Gaussian with $\sigma = 0.05$ arcmin.

The background for each data set was estimated from an annulus, the radius of which was chosen so as to place it approximately in the region of lowest flux. Diffuse emission was removed from this annulus by extracting an azimuthal profile and masking regions with a number of counts greater than 4σ above the mean. A background model could then be constructed and subtracted from the data sets.

Point sources within the image were found using maximum likelihood searching and removed to 1.2 times the 95 per cent radius for 0.5 keV photons. The background subtraction and point-source searching were then repeated until the same number of sources were found upon successive iterations. Extended sources, such as background clusters, were manually identified and removed to the radius at which their contribution became approximately equal to the surrounding emission. Extended emission coincident with the BGG has been shown to exhibit properties that correlate with the properties of the surrounding group emission (Helsdon & Ponman 2000a) and is hence best identified with the group rather than the central galaxy. Therefore, we have included any such emission in our analysis. Each

Table 2. The optical data (Section 3). Group membership was calculated using a position/velocity search for each group and a luminosity cut of $L_{\rm cut} = 2.73 \times 10^{41}$ erg s^{-1}. The number of galaxies is given before and after the cut. Groups marked with † have $N_{\rm gal} < 4$ before the cut and have been excluded from the statistical analysis.

Group name	$N_{\rm gal}$		v (km s^{-1})	$\sigma_{\rm v}$ (km s^{-1})	D (Mpc)	r_{500} Mpc)	$\bar{\rho}_{\rm gal}$ (Mpc^{-3})	$L_{\rm B}$ (log L$_\odot$)	$f_{\rm sp}$	$L_{\rm BGG}$ (log L$_\odot$)	L_{12}	$T_{\rm BGG}$
HCG 4†	2	2	8138 ± 146	207 ± 207	115	0.36	10 ± 7	10.85	0.50	10.73	5.45	Late
NGC 315	5	4	5141 ± 173	387 ± 146	72	0.55	6 ± 3	11.19	0.33	11.03	5.25	Early
NGC 383	33	27	5174 ± 8	450 ± 57	73	0.69	20 ± 4	11.54	0.20	10.56	1.22	Early
NGC 524	10	10	2470 ± 55	175 ± 42	35	0.45	26 ± 8	11.01	0.40	10.77	9.46	Early
NGC 533	28	21	5413 ± 3	439 ± 60	76	0.58	25 ± 6	11.52	0.55	10.99	1.14	Early
HCG 10	5	5	4843 ± 103	231 ± 87	68	0.24	84 ± 38	11.01	0.50	10.60	1.06	Early
NGC 720	4	4	1640 ± 136	273 ± 122	23	0.40	15 ± 7	10.55	0.50	10.46	23.55	Early
NGC 741	33	15	5595 ± 79	453 ± 57	79	0.62	15 ± 4	11.41	0.46	11.11	8.09	Early
HCG 15	7	7	6742 ± 153	404 ± 122	95	0.54	11 ± 4	10.85	0.43	10.26	1.15	Early
HCG 16	7	6	3956 ± 30	80 ± 24	57	0.32	45 ± 18	10.95	0.83	10.44	1.58	Late
NGC 1052	5	4	1366 ± 41	91 ± 35	20	0.36	21 ± 10	10.37	0.50	9.97	1.47	Early
HCG 22	4	4	2599 ± 13	25 ± 11	39	0.29	40 ± 20	10.57	0.25	10.42	9.12	Early
NGC 1332	10	9	1489 ± 59	186 ± 45	23	0.42	29 ± 10	10.55	0.56	10.06	1.42	Early
NGC 1407	20	18	1682 ± 71	319 ± 52	26	0.57	24 ± 6	11.05	0.33	10.74	5.55	Early
NGC 1566	9	9	1402 ± 61	184 ± 47	21	0.47	21 ± 7	11.27	0.33	10.70	1.43	Late
NGC 1587	7	6	3671 ± 43	115 ± 35	55	0.55	9 ± 4	11.07	0.40	10.60	1.10	Early
NGC 1808	4	4	1071 ± 52	104 ± 47	17	0.32	29 ± 15	10.73	1.00	10.35	1.11	Late
NGC 2563	32	31	4688 ± 68	384 ± 49	73	0.57	39 ± 7	11.45	0.53	10.63	1.80	Early
HCG 40	6	6	6596 ± 64	157 ± 52	102	0.45	16 ± 6	11.08	0.33	10.71	3.10	Early
HCG 42	23	19	3801 ± 59	282 ± 43	64	0.48	40 ± 9	11.33	0.36	10.95	5.40	Early
NGC 3227	6	5	1265 ± 69	169 ± 56	27	0.34	29 ± 13	10.80	0.80	10.60	3.02	Late
HCG 48	4	2	2587 ± 158	316 ± 141	41	0.23	39 ± 28	10.39	0.50	9.44	n/a	Late
NGC 3396	12	11	1595 ± 31	106 ± 23	31	0.48	24 ± 7	10.89	1.00	10.22	1.24	Late
NGC 3557	14	11	2858 ± 80	300 ± 60	39	0.27	132 ± 40	11.12	0.40	10.82	4.33	Early
NGC 3607	13	11	1099 ± 78	280 ± 58	23	0.33	72 ± 22	11.02	0.33	10.61	2.25	Early
NGC 3640	8	7	1509 ± 75	211 ± 59	29	0.35	37 ± 14	10.83	0.43	10.56	4.17	Early
NGC 3665	4	3	2043 ± 43	87 ± 39	37	0.38	13 ± 7	10.81	0.00	10.62	3.40	Early
NGC 3783†	1	1	2917	n/a	36	0.25	n/a	10.29	1.00	10.25	n/a	Late
HCG 58	7	7	6269 ± 70	184 ± 55	98	0.51	12 ± 5	11.23	0.67	10.59	1.18	Late
NGC 3923	8	4	1764 ± 85	239 ± 66	22	0.40	15 ± 7	10.80	0.50	10.54	2.58	Early
NGC 4065	13	13	6880 ± 125	450 ± 94	106	0.62	13 ± 4	11.57	0.31	10.81	1.41	Early
NGC 4073	32	31	6042 ± 100	565 ± 72	96	0.69	22 ± 4	11.70	0.13	11.19	4.57	Early
NGC 4151	6	4	1023 ± 42	102 ± 34	23	0.29	38 ± 19	10.62	1.00	10.31	1.29	Late
NGC 4193	7	6	2159 ± 76	202 ± 61	39	0.39	24 ± 10	10.93	0.83	10.11	3.02	Late
NGC 4261	29	25	2332 ± 37	197 ± 27	41	0.64	23 ± 5	11.47	0.21	10.86	2.17	Early
NGC 4325	16	16	7632 ± 94	376 ± 70	117	0.51	29 ± 7	11.06	0.20	10.61	1.53	Early
NGC 4589	10	9	1640 ± 90	284 ± 69	29	0.43	26 ± 9	10.69	0.67	10.15	1.25	Early
NGC 4565†	2	2	1318 ± 50	71 ± 71	27	0.34	13 ± 9	10.93	1.00	10.87	27.04	Late
NGC 4636	9	4	936 ± 95	284 ± 73	10	0.51	7 ± 4	10.45	0.00	10.04	1.07	Early
NGC 4697	6	5	1404 ± 49	120 ± 40	20	0.32	38 ± 17	10.88	0.75	10.74	5.06	Early
NGC 4725	4	2	1228 ± 25	49 ± 22	25	0.40	8 ± 5	11.02	1.00	10.95	13.80	Late
HCG 62	35	33	4291 ± 71	418 ± 51	74	0.67	26 ± 5	11.50	0.33	10.54	1.20	Early
NGC 5044	18	18	2518 ± 100	426 ± 74	33	0.62	18 ± 4	11.18	0.31	10.50	1.43	Early
NGC 5129	23	23	7012 ± 71	342 ± 52	108	0.51	40 ± 8	11.54	0.60	11.05	2.31	Early
NGC 5171	14	12	6924 ± 132	494 ± 99	107	0.58	15 ± 4	11.28	0.00	10.76	2.65	Early
HCG 67	10	10	7455 ± 83	261 ± 63	115	0.46	24 ± 8	11.32	0.60	10.94	4.29	Early
NGC 5322	5	3	2032 ± 74	166 ± 63	35	0.27	37 ± 22	10.90	0.33	10.82	22.08	Early
HCG 68	17	16	2407 ± 46	191 ± 34	41	0.43	50 ± 12	11.41	0.67	10.64	1.19	Early
NGC 5689	5	4	2240 ± 36	80 ± 30	38	0.26	57 ± 29	10.48	0.75	9.51	1.74	Late
NGC 5846	25	14	1866 ± 69	346 ± 51	30	0.48	30 ± 8	11.24	0.27	10.72	1.57	Early
NGC 5907	6	3	768 ± 29	72 ± 24	17	0.24	50 ± 29	10.42	1.00	10.23	2.75	Late
NGC 5930	4	4	2500 ± 75	150 ± 67	41	0.55	6 ± 2	10.32	1.00	9.98	1.58	Late
NGC 6338	37	36	8789 ± 107	651 ± 77	127	0.88	13 ± 2	11.80	0.44	11.05	1.37	Early
NGC 6574†	2	1	2266 ± 21	29 ± 29	35	0.16	56 ± 56	10.00	1.00	9.96	n/a	Late
NGC 7144†	2	2	1912 ± 29	41 ± 41	27	0.41	7 ± 5	10.65	0.00	10.36	1.37	Early
HCG 90	15	9	2559 ± 34	131 ± 25	36	0.38	39 ± 13	10.87	0.62	10.37	1.60	Early
HCG 92	5	5	6347 ± 209	467 ± 176	88	0.47	11 ± 5	11.06	0.40	10.52	1.19	Late
IC 1459	8	7	1835 ± 79	223 ± 62	26	0.35	39 ± 15	10.93	0.86	10.62	3.40	Early
NGC 7714†	2	2	2784 ± 20	28 ± 28	39	0.22	48 ± 34	10.30	1.00	10.17	4.70	Late
HCG 97	14	14	6638 ± 114	425 ± 85	92	0.51	26 ± 7	11.07	0.50	10.39	1.15	Early

Table 3. Results of the spatial analysis (Section 4.1). Groups marked with † have $N_{\mathrm{gal}} < 4$ before the luminosity cut and have been excluded from the statistical analysis.

Group name	Extended r_{core} (kpc)	Extended β_{fit}	Extended e	Central r_{core} (kpc)	Central β_{fit}
HCG 4†	n/a	n/a	n/a	n/a	n/a
NGC 315	n/a	n/a	n/a	n/a	n/a
NGC 383	2.11 ± 0.21	0.36 ± 0.00	1.08 ± 0.03	0.41 ± 0.43	0.60 ± 0.15
NGC 524	n/a	n/a	n/a	n/a	n/a
NGC 533	2.21 ± 1.68	0.42 ± 0.01	1.50 ± 0.03	2.52 ± 0.83	0.59 ± 0.06
HCG 10	n/a	n/a	n/a	n/a	n/a
NGC 720	1.15 ± 0.20	0.47 ± 0.01	1.21 ± 0.06	n/a	n/a
NGC 741	2.30 ± 0.18	0.44 ± 0.01	1.30 ± 0.09	n/a	n/a
HCG 15	n/a	n/a	n/a	n/a	n/a
HCG 16	n/a	n/a	n/a	n/a	n/a
NGC 1052	n/a	n/a	n/a	n/a	n/a
HCG 22	1.34 ± 4.75	0.44 ± 0.20	1.37 ± 0.77	n/a	n/a
NGC 1332	0.07 ± 0.16	0.52 ± 0.01	1.19 ± 0.12	n/a	n/a
NGC 1407	0.08 ± 0.15	0.46 ± 0.01	1.22 ± 0.06	n/a	n/a
NGC 1566	n/a	n/a	n/a	n/a	n/a
NGC 1587	4.34 ± 4.34	0.46 ± 0.09	1.26 ± 0.45	n/a	n/a
NGC 1808	n/a	n/a	n/a	n/a	n/a
NGC 2563	2.14 ± 0.12	0.37 ± 0.01	1.26 ± 0.06.	n/a	n/a
HCG 40	n/a	n/a	n/a	n/a	n/a
HCG 42	4.69 ± 0.72	0.56 ± 0.02	1.29 ± 0.08	n/a	n/a
NGC 3227	0.77 ± 0.60	0.57 ± 0.02	1.21 ± 0.09	n/a	n/a
HCG 48	1.20 ± 1.56	0.48 ± 0.02	1.62 ± 0.30	n/a	n/a
NGC 3396	n/a	n/a	n/a	n/a	n/a
NGC 3557	1.13 ± 0.21	0.52 ± 0.03	1.93 ± 0.34	n/a	n/a
NGC 3607	1.98 ± 0.93	0.39 ± 0.02	2.06 ± 0.18	5.16 ± 2.73	0.60 ± 0.21
NGC 3640	0.08 ± 0.19	0.43 ± 0.05	2.31 ± 0.84	n/a	n/a
NGC 3665	1.08 ± 1.31	0.47 ± 0.03	1.67 ± 0.40	n/a	n/a
NGC 3783†	n/a	n/a	n/a	n/a	n/a
HCG 58	n/a	n/a	n/a	n/a	n/a
NGC 3923	0.63 ± 0.06	0.55 ± 0.01	1.18 ± 0.08	n/a	n/a
NGC 4065	3.08 ± 0.51	0.36 ± 0.01	2.75 ± 0.35	6.68 ± 7.86	0.37 ± 0.03
NGC 4073	9.42 ± 2.89	0.43 ± 0.01	1.20 ± 0.03	3.72 ± 1.50	0.53 ± 0.07
NGC 4151	n/a	n/a	n/a	n/a	n/a
NGC 4193	n/a	n/a	n/a	n/a	n/a
NGC 4261	40.08 ± 12.01	0.44 ± 0.09	1.17 ± 0.12	3.31 ± 1.26	1.17 ± 0.44
NGC 4325	27.56 ± 4.97	0.58 ± 0.01	1.16 ± 0.05	n/a	0.49 ± 0.03
NGC 4589	9.33 ± 0.83	0.52 ± 0.07	2.65 ± 0.39	3.41 ± 2.04	n/a
NGC 4565†	n/a	n/a	n/a	n/a	n/a
NGC 4636	0.30 ± 0.06	0.47 ± 0.00	1.08 ± 0.02	2.67 ± 0.25	0.79 ± 0.04
NGC 4697	1.25 ± 0.29	0.46 ± 0.02	1.37 ± 0.10	n/a	n/a
NGC 4725	n/a	n/a	n/a	n/a	n/a
HCG 62	2.44 ± 0.26	0.48 ± 0.01	1.12 ± 0.03	10.75 ± 0.60	1.00 ± 0.05
NGC 5044	5.96 ± 0.16	0.51 ± 0.00	1.04 ± 0.01	11.04 ± 0.66	0.80 ± 0.06
NGC 5129	3.14 ± 1.71	0.43 ± 0.02	1.18 ± 0.18	n/a	n/a
NGC 5171	n/a	n/a	n/a	n/a	n/a
HCG 67	4.77 ± 1.57	0.54 ± 0.07	3.16 ± 0.05	n/a	n/a
NGC 5322	n/a	n/a	n/a	n/a	n/a
HCG 68	5.97 ± 3.43	0.45 ± 0.05	1.63 ± 0.07	n/a	n/a
NGC 5689	n/a	n/a	n/a	n/a	n/a
NGC 5846	2.19 ± 0.26	0.51 ± 0.01	1.13 ± 0.04	n/a	n/a
NGC 5907	n/a	n/a	n/a	n/a	n/a
NGC 5930	n/a	n/a	n/a	n/a	n/a
NGC 6338	3.72 ± 0.98	0.44 ± 0.01	1.30 ± 0.05	10.32 ± 4.35	0.86 ± 0.34
NGC 6574†	n/a	n/a	n/a	n/a	n/a
NGC 7144†	0.77 ± 1.41	0.45 ± 0.03	5.03 ± 3.65	n/a	n/a
HCG 90	0.91 ± 1.54	0.41 ± 0.03	1.69 ± 0.26	3.89 ± 1.12	1.00 ± 0.20
HCG 92	n/a	n/a	n/a	n/a	n/a
IC 1459	0.74 ± 2.26	0.45 ± 0.02	1.26 ± 0.07	n/a	n/a
NGC 7714†	n/a	n/a	n/a	n/a	n/a
HCG 97	2.73 ± 3.06	0.44 ± 0.01	1.53 ± 0.13	4.31 ± 1.22	0.50 ± 0.03

Table 4. The spectral data (Section 4.2). The above parameters are derived from an absorbed MEKAL hot plasma model that we have fitted to 52 of our 60 data sets. Luminosities shown without corresponding values of temperature or metal abundance have been derived from fixed models, with $T_X = 1$ and $Z = 0.3$. Groups marked with † have $N_{gal} < 4$ before the luminosity cut and have been excluded from the statistical analysis. The final column indicates the subsample to which the group belongs (Section 2) and those marked with *have been manually altered from their default classification.

Group name	T_X (kev)	Z ($Z_{\odot}$)	$\log L_X$ (erg s^{-1})	$\log L_X(r_{500})$ (erg s^{-1})	$\log L_X/L_B$ (erg s^{-1} $L_{\odot}^{-1}$)	β_{spec} (°)	(kpc)	r_{cut} (10^{21} cm^{-2})	N_H	Sample
HCG 4†	n/a	n/a	41.48 ± 0.19	41.62 ± 0.19	30.64 ± 0.19	n/a	0.06	120	0.15	G
NGC 315	0.97 ± 0.22	0.30 ± 0.98	41.21 ± 0.10	41.41 ± 0.10	30.02 ± 0.10	0.46 ± 0.43	0.08	98	0.59	G
NGC 383	1.51 ± 0.06	0.42 ± 0.08	43.07 ± 0.01	43.10 ± 0.01	31.53 ± 0.01	0.84 ± 0.22	0.50	633	0.54	G
NGC 524	0.65 ± 0.07	0.22 ± 0.15	41.05 ± 0.05	41.33 ± 0.05	30.03 ± 0.05	0.30 ± 0.15	0.09	56	0.48	H
NGC 533	1.08 ± 0.05	0.68 ± 0.23	42.67 ± 0.03	42.73 ± 0.03	31.16 ± 0.03	1.12 ± 0.31	0.28	372	0.31	G
HCG 10	0.19 ± 0.07	0.00 ± 0.01	41.70 ± 0.14	41.82 ± 0.14	30.69 ± 0.14	1.79 ± 1.51	0.08	95	0.50	G
NGC 720	0.52 ± 0.03	0.18 ± 0.02	41.20 ± 0.02	41.43 ± 0.02	30.65 ± 0.02	0.90 ± 0.80	0.16	65	0.15	G
NGC 741	1.21 ± 0.09	2.00 ± 0.67	42.44 ± 0.06	42.50 ± 0.06	31.03 ± 0.06	1.07 ± 0.28	0.28	386	0.44	G
HCG 15	0.93 ± 0.13	0.05 ± 0.03	42.12 ± 0.05	42.25 ± 0.05	31.26 ± 0.05	1.10 ± 0.68	0.10	166	0.32	G
HCG 16	0.32 ± 0.07	0.13 ± 0.13	41.30 ± 0.11	41.43 ± 0.11	30.35 ± 0.11	0.12 ± 0.08	0.12	119	0.22	G
NGC 1052	0.41 ± 0.15	0.00 ± 0.02	40.08 ± 0.15	40.53 ± 0.15	29.70 ± 0.15	0.13 ± 0.11	0.07	25	0.31	H
HCG 22	0.26 ± 0.04	2.00 ± 0.51	40.68 ± 0.13	41.03 ± 0.13	30.11 ± 0.13	0.01 ± 0.01	0.07	47	0.42	G*
NGC 1332	0.56 ± 0.03	0.15 ± 0.03	40.81 ± 0.02	40.93 ± 0.02	30.27 ± 0.02	0.39 ± 0.19	0.07	28	0.22	H
NGC 1407	1.02 ± 0.04	0.23 ± 0.05	41.69 ± 0.02	41.92 ± 0.02	30.64 ± 0.02	0.62 ± 0.20	0.23	105	0.54	G
NGC 1566	0.70 ± 0.11	0.00 ± 0.02	40.41 ± 0.05	40.85 ± 0.05	29.14 ± 0.05	0.30 ± 0.16	0.08	29	0.13	H
NGC 1587	0.96 ± 0.17	0.47 ± 1.24	41.18 ± 0.09	41.53 ± 0.09	30.11 ± 0.09	0.09 ± 0.05	0.08	77	0.68	G
NGC 1808	n/a	n/a	<40.10	<40.59	<29.37	n/a	0.07	21	0.27	U
NGC 2563	1.05 ± 0.04	0.64 ± 0.20	42.50 ± 0.03	42.66 ± 0.03	31.05 ± 0.03	0.88 ± 0.23	0.28	359	0.42	G
HCG 40	n/a	n/a	<41.04	<41.30	<29.96	n/a	0.04	64	0.35	U
HCG 42	0.75 ± 0.04	0.29 ± 0.10	41.99 ± 0.02	42.07 ± 0.02	30.66 ± 0.02	0.67 ± 0.21	0.10	112	0.48	G
NGC 3227	n/a	n/a	41.23 ± 0.05	41.28 ± 0.05	30.43 ± 0.05	n/a	0.12	56	0.21	H
HCG 48	n/a	n/a	41.09 ± 0.04	41.30 ± 0.04	29.65 ± 0.08	n/a	0.06	43	0.51	G
NGC 3396	0.74 ± 0.14	0.15 ± 0.10	40.53 ± 0.08	40.99 ± 0.08	30.70 ± 0.04	0.10 ± 0.04	0.05	27	0.20	H
NGC 3557	0.24 ± 0.02	0.00 ± 0.01	42.04 ± 0.04	42.11 ± 0.04	30.93 ± 0.04	2.40 ± 0.98	0.14	95	0.74	G
NGC 3607	0.35 ± 0.04	0.23 ± 0.10	41.05 ± 0.05	41.50 ± 0.05	30.02 ± 0.05	1.40 ± 0.60	0.15	62	0.15	G
NGC 3640	n/a	n/a	<40.37	<40.74	<29.54	n/a	0.11	55	0.43	U
NGC 3665	0.47 ± 0.10	0.17 ± 0.14	41.11 ± 0.08	41.32 ± 0.08	30.30 ± 0.08	0.10 ± 0.09	0.11	71	0.21	G
NGC 3783†	n/a	n/a	40.76 ± 0.11	40.94 ± 0.11	30.46 ± 0.11	n/a	0.11	69	0.85	G
HCG 58	n/a	n/a	<41.33	<41.50	<30.11	n/a	0.07	120	0.32	U
NGC 3923	0.52 ± 0.03	0.18 ± 0.05	40.98 ± 0.02	41.07 ± 0.02	30.18 ± 0.02	0.69 ± 0.38	0.09	34	0.62	H
NGC 4065	1.22 ± 0.08	0.97 ± 0.48	42.64 ± 0.05	42.78 ± 0.05	31.08 ± 0.05	1.04 ± 0.44	0.23	425	0.24	G
NGC 4073	1.52 ± 0.09	0.70 ± 0.15	43.41 ± 0.02	43.48 ± 0.02	31.71 ± 0.02	1.32 ± 0.34	0.28	470	0.19	G
NGC 4151	n/a	n/a	<40.20	<40.51	<29.58	n/a	0.10	40	0.20	U
NGC 4193	n/a	n/a	40.63 ± 0.08	41.06 ± 0.08	29.70 ± 0.08	n/a	0.04	27	0.26	H
NGC 4261	1.30 ± 0.07	1.23 ± 0.42	41.92 ± 0.03	42.30 ± 0.03	30.46 ± 0.03	0.19 ± 0.05	0.18	112	0.15	G
NGC 4325	0.82 ± 0.02	0.50 ± 0.08	43.15 ± 0.01	43.18 ± 0.01	32.09 ± 0.01	1.08 ± 0.40	0.15	307	0.22	G
NGC 4589	0.60 ± 0.07	0.08 ± 0.03	41.61 ± 0.05	41.84 ± 0.05	30.92 ± 0.05	0.84 ± 0.42	0.24	122	0.29	G
NGC 4565†	0.36 ± 0.14	0.10 ± 0.15	40.44 ± 0.14	40.74 ± 0.14	29.51 ± 0.14	0.09 ± 0.18	0.10	46	0.13	H
NGC 4636	0.84 ± 0.02	0.41 ± 0.05	41.49 ± 0.02	41.71 ± 0.02	31.04 ± 0.02	0.60 ± 0.31	0.30	68	0.18	G
NGC 4697	0.32 ± 0.03	0.07 ± 0.02	41.01 ± 0.02	41.30 ± 0.02	30.13 ± 0.02	0.28 ± 0.19	0.15	53	0.21	H
NGC 4725	0.50 ± 0.07	0.00 ± 0.01	40.63 ± 0.06	41.08 ± 0.06	29.61 ± 0.06	0.03 ± 0.03	0.06	26	0.10	H
HCG 62	1.43 ± 0.08	2.00 ± 0.56	43.14 ± 0.04	43.20 ± 0.04	31.63 ± 0.04	0.77 ± 0.19	0.22	282	0.30	G
NGC 5044	1.21 ± 0.02	0.69 ± 0.06	43.01 ± 0.01	43.09 ± 0.01	31.82 ± 0.01	0.94 ± 0.33	0.30	180	0.49	G
NGC 5129	0.84 ± 0.06	0.66 ± 0.28	42.33 ± 0.04	42.60 ± 0.04	30.79 ± 0.04	0.87 ± 0.27	0.08	151	0.18	G
NGC 5171	1.07 ± 0.09	1.47 ± 1.25	42.38 ± 0.06	42.45 ± 0.06	31.11 ± 0.06	1.43 ± 0.59	0.16	298	0.19	G
HCG 67	0.68 ± 0.08	0.22 ± 0.13	42.02 ± 0.07	42.07 ± 0.07	30.70 ± 0.07	0.63 ± 0.31	0.11	222	0.25	G
NGC 5322	0.23 ± 0.07	0.00 ± 0.02	40.71 ± 0.10	41.00 ± 0.10	29.82 ± 0.10	0.76 ± 0.62	0.07	43	0.18	H
HCG 68	0.58 ± 0.06	0.09 ± 0.02	41.52 ± 0.04	41.77 ± 0.04	30.12 ± 0.04	0.40 ± 0.15	0.17	122	0.10	G
NGC 5689	n/a	n/a	<40.24	<40.53	<29.76	n/a	0.06	40	0.20	U
NGC 5846	0.73 ± 0.02	1.25 ± 0.69	41.90 ± 0.02	42.04 ± 0.02	30.66 ± 0.02	1.02 ± 0.30	0.18	94	0.43	G
NGC 5907	n/a	n/a	39.69 ± 0.14	40.34 ± 0.14	29.27 ± 0.14	n/a	0.04	12	0.14	H
NGC 5930	0.97 ± 0.27	0.17 ± 0.12	40.73 ± 0.07	41.19 ± 0.07	30.42 ± 0.07	0.14 ± 0.14	0.04	29	0.20	H
NGC 6338	n/a	n/a	43.51 ± 0.02	43.57 ± 0.02	31.72 ± 0.02	n/a	0.28	619	0.26	G
NGC 6574†	n/a	n/a	<40.81	<40.96	<30.81	n/a	0.10	61	1.08	U
NGC 7144†	0.53 ± 0.20	0.00 ± 0.02	40.33 ± 0.13	40.71 ± 0.13	29.69 ± 0.13	0.02 ± 0.04	0.10	46	0.28	H
HCG 90	0.46 ± 0.06	0.08 ± 0.03	41.49 ± 0.05	41.79 ± 0.05	30.62 ± 0.05	0.23 ± 0.09	0.16	101	0.16	G
HCG 92	0.71 ± 0.06	0.20 ± 0.13	41.99 ± 0.04	42.19 ± 0.04	30.93 ± 0.04	1.92 ± 1.46	0.06	93	0.80	G
IC 1459	0.39 ± 0.04	0.04 ± 0.01	41.28 ± 0.04	41.46 ± 0.04	30.35 ± 0.04	0.80 ± 0.45	0.27	121	0.12	G
NGC 7714†	n/a	n/a	<40.03	<40.48	<29.73	n/a	0.03	20	0.49	U
HCG 97	0.82 ± 0.06	0.23 ± 0.10	42.37 ± 0.05	42.43 ± 0.05	31.30 ± 0.05	1.38 ± 0.56	0.21	339	0.36	G

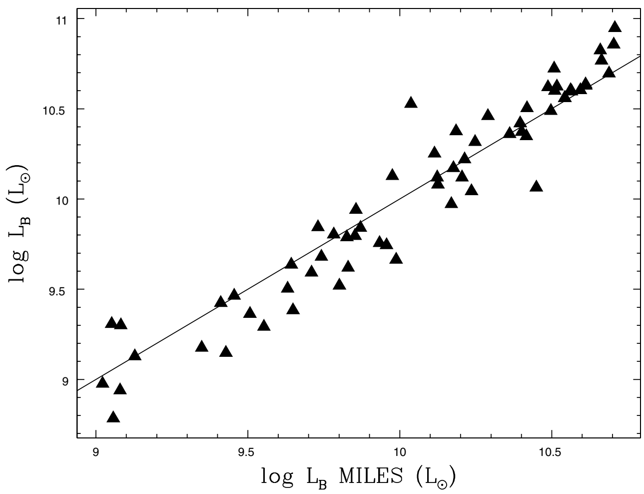

Figure 1. A comparison between our galaxy luminosities and those of Miles et al. (2004). The solid line represents equality.

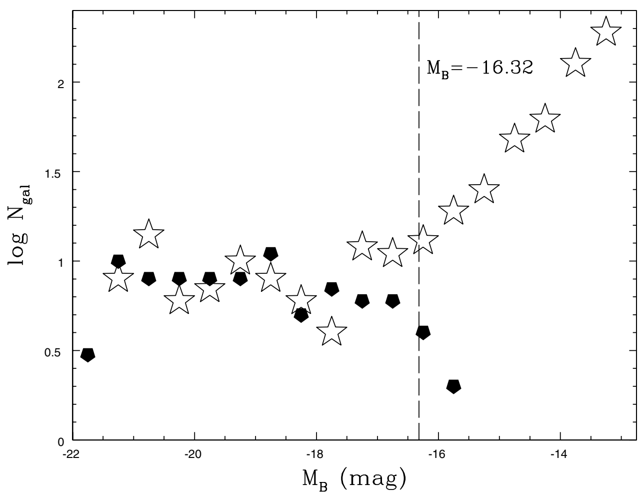

Figure 2. A comparison between our galaxy luminosity function (filled pentagons) and that of Miles et al. (2004) (open stars), for the subset of GEMS groups covered by the latter study. The dashed line represents the luminosity cut at $M_{\rm B} = -16.32$.

exposure was further corrected for dead time effects, vignetting and the shadow formed by the mirror shell support ring and finally divided by the exposure time to produce a map of spectral flux.

4.1 Spatial analysis

On completion of the data reduction, a radial profile centred on the group position was examined and the radius at which the group emission fell to the background level was used to define an extent radius ($r_{\rm ext}$) and hence a radius ($r_{\rm cut}$) from within which X-ray data are extracted for analysis. The $r_{\rm cut}$ radii are given in Table 4. In the case of HCG 48, $r_{\rm ext}$ included emission from the nearby cluster Abell 1060 and we have therefore reduced $r_{\rm cut}$ to a value that only includes regions in which the group emission dominates over the cluster emission. In all other detected groups, $r_{\rm cut} = r_{\rm ext}$. In cases where no emission was evident, an $r_{\rm cut}$ value of 50 kpc was used to calculate upper limits. The number of source counts within this region was then calculated by subtracting the background contribution, as predicted by the background model. In cases where the number of source counts was greater than 3σ above background, the data set was deemed to contain detected X-ray emission.

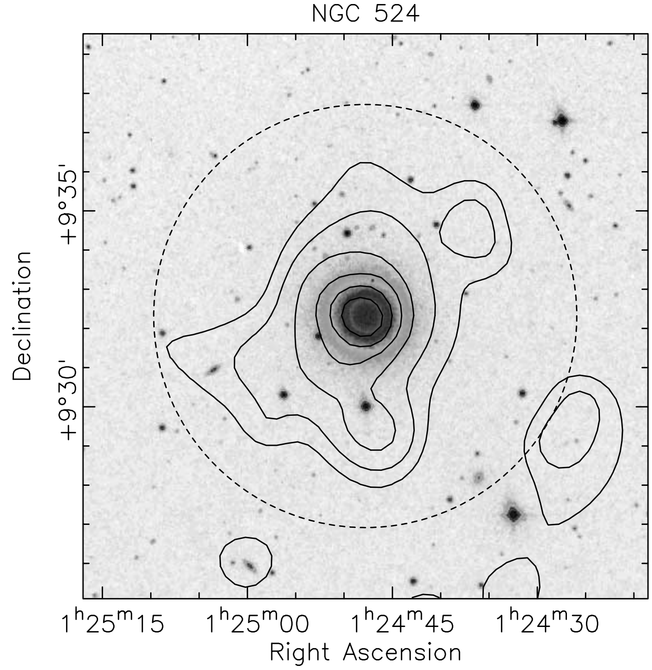

Figure 3. *ROSAT* PSPC contours for NGC 524 overlaid on an optical DSS image. The dashed circle represents $r_{\rm cut} = 56$ kpc. This system has rather compact X-ray emission that we classify as a galaxy halo (H-sample).

It was often useful during the course of this data reduction to examine images of the groups in question. Quantitative results, such as the emission radii calculated in Section 4, could be examined and confirmed using such images. Therefore, we have produced optical images, with X-ray contours overlaid, for all of the groups in our sample. Background variance maps were created assuming Poissonian statistics, smoothed in the usual way and divided into smoothed images to produce significance maps. Contours were drawn on at 5×2^n sigma above the background (n = 0, 1...10) and overlaid on to optical images taken from the Digitised Sky Survey (DSS). Fig. 3 shows an X-ray/optical overlay of NGC 524, which has $r_{\rm cut} =$ 56 kpc (represented by the dashed circle) and, as such, is identified with emission from a galactic halo. NGC 533 (Fig. 4) has $r_{\rm cut} = 372$ kpc indicating group-scale emission.

We have sought to characterize the surface brightness properties of our sample of groups by fitting their emission with a two-dimensional β model, of the form

$$S(r) = S_0 \left[1 + \left(\frac{r}{r_{\rm core}}\right)^2\right]^{-3\beta_{\rm fit}+0.5}. \qquad (6)$$

It has been shown that fitting such a profile in one dimension can lead to an overestimate of the $\beta_{\rm fit}$ parameter in systems with particularly elongated or offset components (Helsdon & Ponman 2000a). An image in the band 0.5 to 2 keV was extracted from all data sets containing a detection and data outside $r_{\rm cut}$ was removed. Remaining data were then fitted with a single-component β model.

Models were convolved with the point spread function (PSF) at an energy determined from the mean photon energy of the data and with free parameters: the central surface brightness S_0, core radius ($r_{\rm core}$), slope ($\beta_{\rm fit}$) and the coordinates of the centre of emission. We

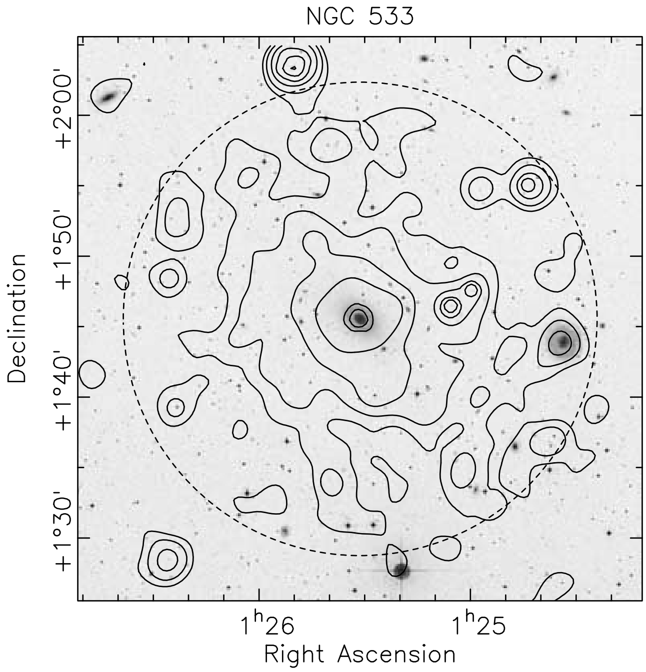

Figure 4. *ROSAT* PSPC contours for NGC 533 overlaid on an optical DSS image. The dashed circle represents $r_{\rm cut} = 372$ kpc. This extensive hot halo is clearly associated with the group as a whole (G-sample).

also allowed our fits to be elliptical by introducing the axis ratio (e) and position angle as additional free parameters.

In cases where a single-component β model was inadequate in describing the emission, a second component was added to the model. Such an inadequacy was identified by examining a radial profile for each group in the G-sample and looking for a shoulder in which the single β model significantly departed from the data. In marginal cases, a fit using the two-component model was attempted. In order to limit the number of free parameters in our two-component fits, we have fixed the axis ratio and position angle of the central component, thus constraining it to be circular.

Surface brightness models were used to correct bolometric fluxes for the removal of point sources and other contamination. For each group the fitted β model (two-component where available) was taken and used to generate a model image from which a count rate was extracted. Regions of contamination, as defined in Section 4, were then removed and the reduced count rate combined with the original count rate to derive a correction factor for the luminosity. Groups with no fitted β model were corrected by taking an image with the regions removed and patching over the holes using a local mean. A correction factor was obtained and applied in the same way. Results of the spatial analysis are presented in Table 3.

4.2 Spectral analysis

We have performed a spectral analysis for all pointings containing a detected galaxy group. A spectrum was obtained by removing all data outside $r_{\rm cut}$ and projecting the cube along its spatial axes. Each spectrum was then fitted with a single-component MEKAL hot plasma model (Mewe, Lemen & van den Oord 1986) and a multiplicative absorption component with the neutral hydrogen column density fixed at a value taken from H I radio observations (Dickey & Lockman 1990).

A spectral fit was considered reliable if the error on the temperature was less than the fitted value of temperature. Where this was not the case, the value of metal abundance was fixed at 0.3 $Z_\odot$ and the fitting repeated. If the fit remained unreliable then the value of temperature was fixed at 1 keV and the normalization fitted. Unabsorbed bolometric fluxes were obtained from all spectral models by setting the neutral hydrogen column density to zero. We have calculated an upper limit on the flux from undetected groups by taking the same fixed model and fitting the normalization to 3σ above the background level. Values of flux were then converted to luminosities, $L_{\rm X}$, using the optically derived distance, D (Section 3). Results of the spectral analysis are presented in Table 4.

The poor spectral resolution of the *ROSAT* PSPC means that values of metal abundance (Z) can often be misleading, even when the value of temperature is deemed reliable. However, simulations have shown us that fixing this value can bias the fitted temperature by up to approximately 20 per cent. We found that fitting a one-component spectral model to variable temperature emission results in a greatly underestimated metal abundance, whilst still producing a reliable value for temperature.

We have produced simple projected temperature profiles for all groups with sufficiently good statistics. For each group we extracted spectra from concentric annuli of increasing radius from the group position and fitted MEKAL hot plasma models to them. The neutral hydrogen column density was fixed as before, and Z was allowed to vary in cases where the data quality had allowed a global value to be fitted. Spectral profiles including more than three bins and showing a significant drop in temperature in the centre were deemed to demonstrate a cool core. In these cases (nine systems), data within the central cool region were removed and the global spectrum refitted, to derive a cooling-corrected temperature. This correction was found to be small: the average drop in $T_{\rm X}$ being only 4 per cent and lying well within the statistical error of $T_{\rm X}$. In these cases the X-ray luminosity was corrected for any central data excised, using the fitted surface brightness model.

Spectral data were combined with optical data to calculate two compound parameters: the ratio of X-ray luminosity to optical luminosity ($L_{\rm X}/L_{\rm B}$) and the spectral index ($\beta_{\rm spec}$) defined by

$$\beta_{\rm spec} = \frac{\mu\sigma_{\rm v}^2}{kT} = 6.26 \times 10^{-6}\left(\frac{\sigma_{\rm v}^2}{T_{\rm X}}\right), \qquad (7)$$

where μ is the mean particle mass of the gas in kg ($\mu = 0.6\, m_{\rm p}$), $\sigma_{\rm v}$ is the line-of-sight velocity dispersion in km s^{-1}, k is Boltzmann's constant, T is the temperature in K and $T_{\rm X}$ the temperature in keV.

We have used the fitted β models to calculate a luminosity within r_{500} and Fig. 5 shows this extrapolated luminosity [$L_{\rm X}(r_{500})$] plotted against $L_{\rm X}$. Errors in $L_{\rm X}(r_{500})$ plotted in the figure and listed in Table 4 are extrapolated from errors in $L_{\rm X}$, ignoring any errors arising from uncertainties in $r_{\rm core}$ or $\beta_{\rm fit}$. In cases where no fitted β model was available, a standard model with the average values of $r_{\rm core} = 6$ kpc and $\beta_{\rm fit} = 0.5$ (Table 5) was used instead. As expected, the greatest correction to the luminosity occurs within the lowest luminosity systems, where it can be as large as a factor of $\sim$3.

To investigate the impact on $L_{\rm X}(r_{500})$ of errors in $r_{\rm core}$ and $\beta_{\rm fit}$, we performed a full Monte Carlo analysis, incorporating a Gaussian spread in normalization, $r_{\rm core}$ and $\beta_{\rm fit}$, for the system (NGC 720), which has fairly typical parameter values. The total derived error on $L_{\rm X}(r_{500})$ was 8 per cent, a factor of 2 greater than the value of 4 per cent based on the normalization error alone.

4.3 Correlations in properties

We have derived 18 group parameters, listed in Table 5, which we use for our statistical analysis. All parameters were cross-correlated

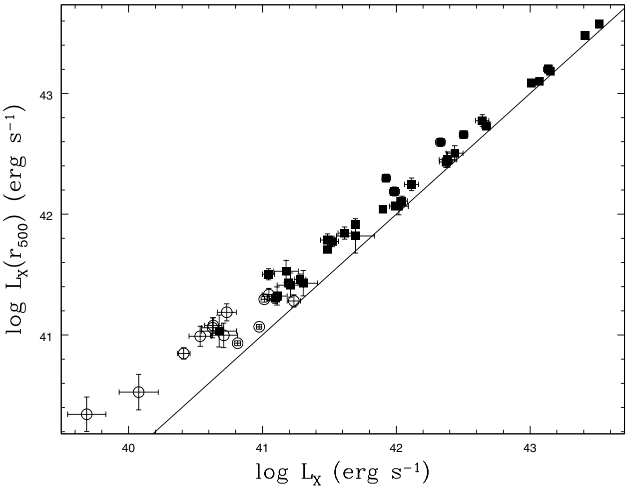

Figure 5. A plot of the luminosity within r_{500} against that within r_{cut}. Filled squares represent the G-sample and open circles the H-sample. The solid line represents equality.

and any significant relationships identified by examining the resulting plots and the Kendall rank correlation coefficient (K), which corresponds to a correlation significance in units of Gaussian sigma. Trends were parametrized by taking the bisector between two orthogonal least-squares regression fits, as calculated by the SLOPES software (Feigelson & Babu 1992). We prefer to use an unweighted orthogonal regression, because the scatter observed in the properties of galaxy groups is primarily non-statistical (Helsdon & Ponman 2000b). Therefore, it is inappropriate to weight points by their statistical errors when fitting regression lines.

The regression parameters are summarized in Table 5 and relationships listed in Table 6. These results are presented and discussed in the following sections. In all figures, filled squares represent X-ray groups (G-sample), open circles X-ray galactic haloes (H-sample) and crosses X-ray non-detections (U-sample).

Table 5. A summary of the parameters investigated in the statistical analysis. N is the number of data points used in each calculation.

Parameter		Mean	Min.	Max.	N
σ_{v}	(km s^{-1})	261	25	651	54
D	(Mpc)	53	10	127	54
r_{500}	(Mpc)	0.46	0.23	0.88	54
$r_{500\sigma}$	(Mpc)	0.45	0.10	1.07	38
$\bar{\rho}_{\mathrm{gal}}$	(Mpc^{-3})	30	6	131	54
L_{B}	(log L$_{\odot}$)	11.16	10.32	11.80	54
f_{sp}		0.50	0.00	1.00	54
L_{BGG}	(log L$_{\odot}$)	10.67	9.44	11.19	54
L_{12}		3.64	1.06	23.55	54
r_{core}	(kpc)	6.47	0.07	81.26	34
β_{fit}		0.47	0.36	0.58	34
e		1.52	1.04	3.16	34
T_{X}	(kev)	0.75	0.19	1.52	43
Z	(Z$_{\odot}$)	0.46	0.00	2.00	43
L_{X}	(log erg s^{-1})	42.47	39.69	43.51	48
$L_{\mathrm{X}}(r_{500})$	(log erg s^{-1})	42.55	40.34	43.57	48
β_{spec}		0.75	0.01	2.40	43
$L_{\mathrm{X}}/L_{\mathrm{B}}$	(log erg s^{-1} L$_{\odot}^{-1}$)	31.07	29.14	32.09	48

Table 6. A summary of the relationships discussed in the following sections. Values of slope and intercept describe an unweighted orthogonal regression fit to all data and the G-sample (bold) and H-sample separately. K is Kendall's rank correlation co-efficient, corresponding to a significance in units of Gaussian sigma.

y	x	**G-Sample**			H-Sample			All			Figure
		Slope	**Intercept**	***K***	Slope	Intercept	K	Slope	Intercept	K	
log L_{X}	log T_{X}	**2.75 ± 0.49**	**42.38 ± 0.10**	**4.37**	−1.05 ± 0.22	40.40 ± 0.11	−0.09	3.22 ± 0.51	42.25 ± 0.11	4.537	12
log L_{X}	log σ_{v}	**2.56 ± 0.66**	**35.73 ± 1.68**	**4.94**	1.90 ± 0.62	36.61 ± 1.37	1.46	3.10 ± 0.43	34.27 ± 1.05	6.854	14
β_{spec}	log L_{X}	**0.84 ± 0.13**	***−34.33± 5.34***	**2.73**	0.86 ± 0.21	−34.80 ± 8.37	0.98	0.69 ± 0.11	−28.14 ± 4.59	4.323	17
log L_{X}	log L_{B}	**2.05 ± 0.21**	**19.13 ± 2.41**	**4.78**	1.28 ± 0.34	26.82 ± 3.66	0.12	2.47 ± 0.19	14.25 ± 2.15	5.978	18
log L_{B}	log T_{X}	**1.28 ± 0.20**	**11.33 ± 0.04**	**3.95**	−1.12 ± 0.31	10.48 ± 0.16	−0.27	1.37 ± 0.17	11.30 ± 0.04	4.055	19
f_{sp}	log T_{X}	***−0.93± 0.11***	**0.26 ± 0.04**	***−2.64***	1.32 ± 0.19	1.01 ± 0.11	0.76	−1.03 ± 0.09	0.27 ± 0.04	−2.554	22
f_{sp}	log σ_{v}	***−0.88± 1.88***	**2.56 ± 4.63**	***−1.78***	−1.28 ± 0.21	3.43 ± 0.45	−1.67	−0.93 ± 0.10	2.68 ± 0.24	−3.918	23
f_{sp}	log L_{X}	***−0.55± 0.22***	**23.47 ± 9.32**	***−1.03***	−0.84 ± 0.21	34.92 ± 8.63	−0.64	−0.34 ± 0.04	14.68 ± 1.87	−3.503	24
f_{sp}	log Z	***−0.53± 0.08***	**0.16 ± 0.06**	***−3.17***	0.36 ± 0.19	1.07 ± 0.17	−0.31	−0.54 ± 0.10	0.13 ± 0.06	−3.877	25
f_{sp}	log $\bar{\rho}_{\mathrm{gal}}$	**0.78 ± 0.09**	***−0.68± 0.13***	**2.53**	−1.00 ± 0.10	2.02 ± 0.16	−0.52	0.98 ± 0.04	−0.85 ± 0.06	1.943	26
log L_{BGG}	log L_{B}	**0.96 ± 0.15**	***−0.08± 1.73***	**4.86**	1.22 ± 0.17	−2.70 ± 1.82	2.68	0.99 ± 0.11	−0.38 ± 1.19	6.236	29
log L_{BGG}	log σ_{v}	**1.09 ± 0.19**	**7.95 ± 0.52**	**1.92**	−1.09 ± 0.38	12.77 ± 0.82	−0.37	1.14 ± 0.14	7.89 ± 0.36	2.772	30

5 COMPARISON WITH PREVIOUS WORK

We compare our derived values of $N_{\rm gal}$ and $\sigma_{\rm v}$ to those given in the group catalogues from which our groups are drawn. Fig. 6 shows a reasonable agreement between values of $N_{\rm gal}$ in all but the compact groups, where we typically find many more galaxy members, because the original compact group search included only a compact core of galaxies in what is generally a much larger group (e.g Zabludoff & Mulchaey 1998). We also find a reasonable match between our values of $\sigma_{\rm v}$ and those taken from the source catalogues (Fig. 7).

The recently published atlas by MDMB includes 109 *ROSAT*-observed groups, larger than the present sample, with X-ray emission detected from 61. X-ray fluxes in this study have not been corrected to r_{500} and optical properties have been drawn from a variety of group catalogues, rather than re-extracted in a uniform manner as in our sample. However, MDMB subject all their groups to a uniform X-ray data analysis similar in many ways to ours, so

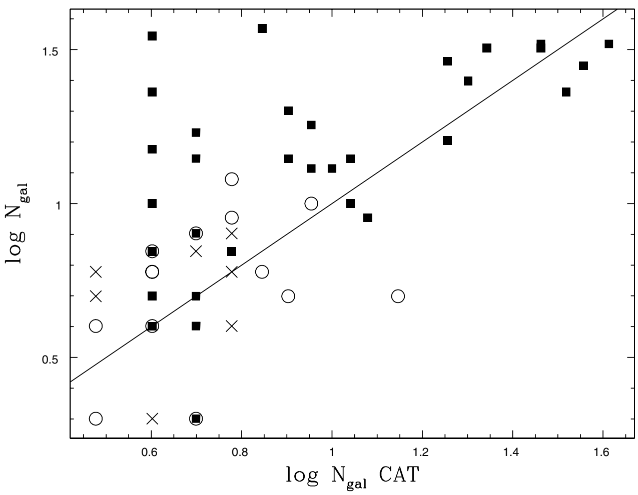

Figure 6. A comparison between our values of $N_{\rm gal}$ and those taken from the source catalogues (Table 1). Filled squares represent the G-sample, open circles the H-sample and crosses non-detections. The solid line represents equality.

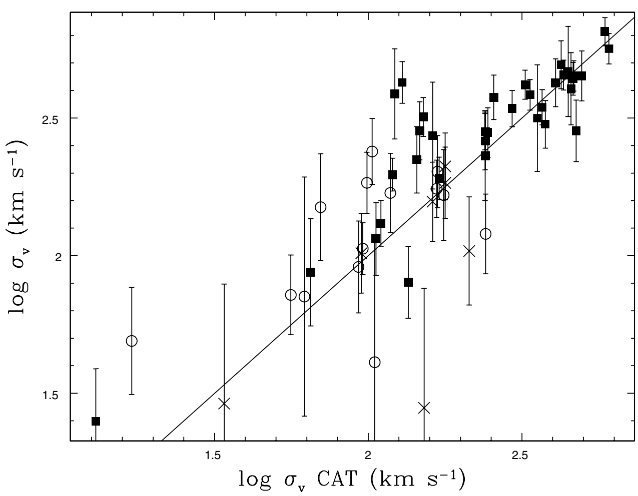

Figure 7. A comparison between our values of $\sigma_{\rm v}$ and those taken from the source catalogues (Table 1). Filled squares represent the G-sample, open circles the H-sample and crosses non-detections. The solid line represents equality.

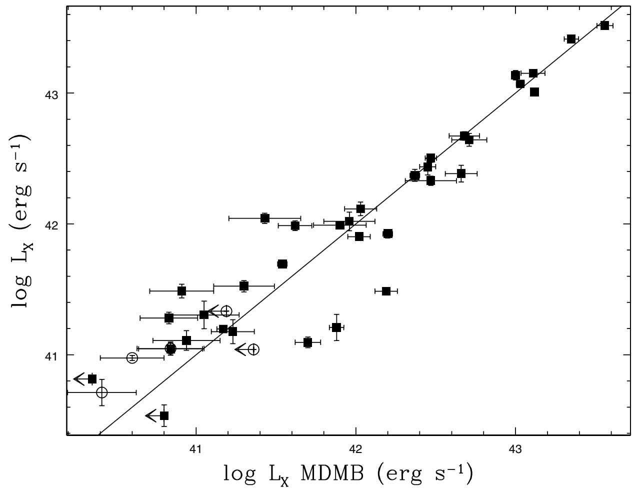

Figure 8. A comparison between our values of $L_{\rm X}$ and those taken from MDMB. Filled squares represent the G-sample, open circles the H-sample and arrows represent upper-limits from non-detections. The solid line represents equality.

that comparisons with our results provide a valuable check. In particular, they adopt the same procedure for choosing $r_{\rm cut}$ and quoted luminosities are bolometric. In the spectral fitting the neutral hydrogen column density is fixed at the galactic value and unconstrained metallicities are fixed at 0.3 solar.

There is an overlap of 43 groups between the two samples. Plotting $L_{\rm X}$ against $L_{\rm X}$ (MDMB) (Fig. 8) shows a good agreement for X-ray bright groups and reasonable agreement amongst groups with lower luminosity, but with a good deal of scatter in the latter. The reason for this scatter is not clear. In general, it appears to be related to neither the radius out to which emission has been integrated in the two studies, nor (see below) the systematic differences in the spectral properties derived. We explored the comparison in more detail for three of the groups for which the disagreement with MDMB was strongest. NGC 315 has a value of $L_{\rm X}$ that is a factor of $\approx$5 less than the MDMB value of $L_{\rm X} = 10^{41.88}$ erg s^{-1}. However, this difference is accounted for by the removal of the central active galactic nucleus (AGN) in our analysis (Section 4). Our $L_{\rm X}$ for HCG 48 is a factor of $\approx$2 less than the MDMB value of $10^{41.70}$ erg s^{-1}. This value has been extracted from a circular region with a value of $r_{\rm cut}$ equivalent to 60 per cent of the MDMB radius of 72 kpc. We have used a smaller radius in order to minimize X-ray contamination from the nearby cluster Abell 1060 and it is this difference that accounts for the deficit in $L_{\rm X}$. NGC 4636 has $L_{\rm X}$ a factor of $\approx$5 less than the MDMB value of $10^{42.19}$ erg s^{-1} and is extracted from a similar size region. Furthermore, the diffuse emission is so extensive that replacing the central AGN only changes the overall $L_{\rm X}$ by a small proportion. The value of $L_{\rm X}$ derived by Helsdon & Ponman (2000a) for the same system is $10^{42.18}$ erg s^{-1}, in good agreement with the MDMB value. However both of these studies take the group velocity from the source catalogue and applying our iterative membership calculation decreases this catalogued value (and hence the distance inferred from it) by a factor of $\sim$2, accounting for the majority of the discrepancy in $L_{\rm X}$. Our value of distance is also in much better agreement with that of the BGG, NGC 4636 ($D = 10$ Mpc).

We find a good agreement between our values of $T_{\rm X}$ and those taken from MDMB (Fig. 9), though the latter have not been corrected for cool cores. Because the MDMB study is based on the same *ROSAT* data that we are using, this comparison does not address

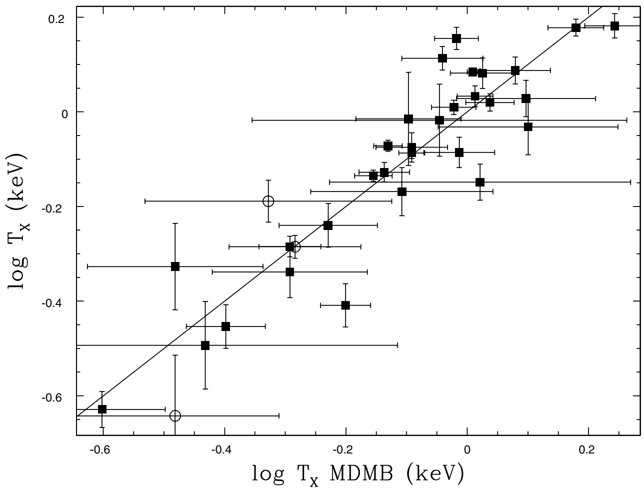

Figure 9. A comparison between our values of T_X and those taken from MDMB. Filled squares represent the G-sample and open circles the H-sample. The solid line represents equality.

the issue of the whether *ROSAT* spectra yield reliable temperatures. The results of Hwang et al. (1999) suggest that for hot plasmas with $T_X > 1.5$ keV, *ROSAT* PSPC temperatures are biased low (by approximately 30 per cent) relative to those derived using the superior spectral capabilities of *ASCA*, whilst for cooler systems temperatures from the two instruments are in reasonable agreement. Because the hottest system in our sample has $T_X = 1.52$ keV, any such bias should have only minor effects on our study.

6 THE RADII OF GALAXY GROUPS

As discussed in Section 3, we have sought in this study to extract group properties within a consistently defined overdensity radius, corresponding to 500 times the critical density of the Universe at the current epoch. The best way to define such a radius for each group would be to derive total mass profiles, to directly measure the radius within which the desired mean density is obtained. This could be done (under the assumption of hydrostatic equilibrium) if gas density and temperature profiles could be extracted from our data. Unfortunately, the quality of the data does not permit reliable gas temperature profiles to be extracted for most of these groups and in no case could such a profile be extended to r_{500}. Failing this, three methods for estimating r_{500} were considered, as described in Section 3, based on the use of X-ray temperature, galaxy velocity dispersion or total optical (blue) luminosity. The principle behind all these, is that a system virializing at $z = 0$ should have a given mean density within its virial radius and hence all overdensity radii should scale as the third power of system mass. Total optical luminosity (L_B) can be used to estimate system mass under the assumption that star formation efficiency (SFE) and mean mass-to-light ratio of galaxies are independent of other group properties.

Unfortunately, these assumptions are debatable. Semi-analytical models of galaxy formation predict a correlation between M/L and halo size. For example, Benson et al. (2000) find that M/L drops by a factor $\sim$3 in their models, between haloes of mass 10^{14} and 10^{12} $M_{\odot}$, i.e. in the group and galaxy regime. Observational evidence on this issue is mixed. Most X-ray studies, such as those by Hradecky et al. (2000) and Sanderson & Ponman (2003), have found the mass-to-light ratio and SFE in groups and clusters to be essentially independent of temperature. However, the study of Hoekstra et al. (2001), based on the weak lensing signal from a set of stacked groups, found M/L lower than that in clusters and a compilation of a variety of measurements on group to cluster scales led Bahcall & Comerford (2002) to conclude that M/L rises gently, as $T_X^{0.3}$, across the temperature range from 1 to 12 keV.

Alternatively, for a system in virial equilibrium, the characteristic velocity dispersion of the galaxies and the gas temperature should be related to system mass via the virial theorem. This leads to

$$T_X \propto \sigma_v^2 \propto M/R \propto M^{2/3}, \tag{8}$$

where the final step involves the assumption of constant mean density for newly virialized systems. Results from cosmological simulations suggest that a scaling relation $M \propto T_X^{1.5}$ can give a robust and reliable measure of mass. Evrard et al. (1996), in an analysis of an ensemble of simulated clusters (including some incorporating feedback), found that mass estimates using a $T_X^{1.5}$ formula with an appropriate normalization, scattered about the true masses, had a standard deviation of only 15 per cent. On the other hand, a number of studies (e.g. Finoguenov, Reiprich & Böhringer 2001) find that the $M-T_X$ relation has a slope steeper than 1.5 and Sanderson et al. (2003) find observational evidence, by comparing X-ray derived masses with the results obtained from simple scaling formulae, that a $T_X^{0.5}$ scaling can overestimate virial radii, especially in cool systems, by up to 40 per cent, leading to a corresponding overestimate in virial mass.

It is known from previous studies (cf. Section 7.3) that the energy per unit mass in gas tends to be higher than that in galaxies (i.e. $\beta_{spec} < 1$) for poor clusters and groups and that in groups there appears to be a great deal of scatter in β_{spec}. This implies that either T_X or σ_v (or both) is an unreliable indicator of system mass. A priori one could think of reasons to suspect either parameter: σ_v is usually statistically poorly determined in groups, as a result of the low number of galaxy redshifts available, and might also be affected by a variety of biases and physical effects, whilst T_X could be vulnerable to the effects which are believed to have raised the entropy of the gas in groups relative to that expected on the basis of what is seen in clusters (Ponman et al. 1999).

To explore this further, we tried both methods (equations 1 and 3) for the evaluation of r_{500} and extracted the group members for each of the two resulting definitions. It is instructive to consider the mean density of galaxies,

$$\bar{\rho}_{gal} = \frac{N_{gal}}{V_{500}} = \frac{N_{gal}}{\frac{4}{3}\pi r_{500}^3}\,\mathrm{Mpc}^{-3}, \tag{9}$$

for the GEMS sample, computed by each method. Histograms showing the distribution of $\bar{\rho}_{gal}$ values obtained are shown in Fig. 10. For comparison, we calculated the expected mean galaxy density within r_{500} from the average Sloan Digital Sky Survey (SDSS) luminosity function of Blanton et al. (2003), by integrating their Schechter function down to our luminosity cut, giving a predicted mean galaxy density

$$\bar{\rho}_{gal}(\mathrm{pred}) = \frac{500}{\Omega_m}\int_{L_{cut}}^{\infty}\phi(L)\,\mathrm{d}L = 27\,\mathrm{Mpc}^{-3}, \tag{10}$$

where Ω_m is the density of ordinary matter, as a fraction of the critical density and is assumed to be 0.3. The predicted mean galaxy density is marked in Figs 10 and 11.

It can be seen that using the T_X-based estimate of r_{500}, the expected density is close to the median of our derived values ($\bar{\rho}_{gal} = 25$), whilst the σ_v-based estimates lead to a much wider scatter in $\bar{\rho}_{gal}$, with some values (mostly for very poor groups) over

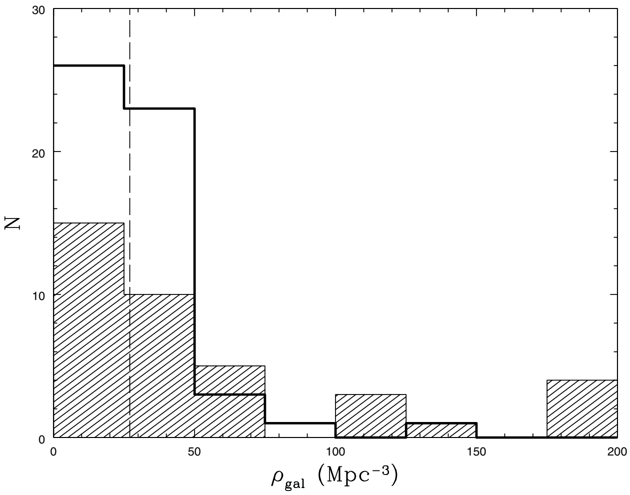

Figure 10. Distribution of mean galaxy densities within r_{500} for the GEMS sample when the r_{500} radii are evaluated using (a) group velocity dispersion (shaded histogram) and (b) X-ray temperature (bold line). The uppermost bin of the $\sigma_{\rm v}$-based histogram contains two groups with much larger densities than indicated ($\bar{\rho}_{\rm gal} = 284$ and 653). The expected mean density of galaxies down to our luminosity cut is shown as a vertical dashed line.

an order of magnitude higher than expected. The standard deviations in the $\bar{\rho}_{\rm gal}$ distributions for the $T_{\rm X}$- and $\sigma_{\rm v}$-based estimates are 21 and 115 Mpc^{-3}, respectively.

In Fig. 11, we compare the derived densities for the two methods, plotted against total optical luminosity of the groups. It can be seen that not only does the $T_{\rm X}$-based analysis give a smaller scatter in $\bar{\rho}_{\rm gal}$, but the inferred densities show no discernable trend with $L_{\rm B}$. It seems that any effects of non-self-similar entropy scaling are not acting to systematically raise $T_{\rm X}$ in lower mass systems, otherwise we would see a trend towards lower apparent $\bar{\rho}_{\rm gal}$ in the poorest systems.

The good agreement between our observed and expected galaxy densities appears to conflict with the conclusions of the Sanderson et al. (2003) analysis, discussed above, because a 40 per cent overestimate in r_{500} would lead to our densities being underestimated by a factor of 2.7, which does not seem consistent with the results shown in Fig. 11. Moreover a number of recent studies (e.g. Nevalainen, Markevitch & Forman 2000; Sato et al. 2000; Finoguenov et al. 2000), have indicated that the $M-T_{\rm X}$ relation for clusters and groups is significantly steeper than the self-similar ($M \propto T_{\rm X}^{1.5}$) relation, although Allen, Schmidt & Fabian (2001) find a relation consistent with self-similarity from a high-quality *Chandra* study of a small sample of rich, relaxed clusters, with a 2500 overdensity radius. If the $M-T_{\rm X}$ relation does have a slope steeper than 1.5, then it follows that the $T_{\rm X}^{0.5}$ scaling for r_{500} is too flat and will presumably tend to overestimate the radius in the group regime.

It should be noted that the good agreement between our median value of galaxy density and the expected value, assumes that galaxies are not biased relative to mass on group scales. Recent results from the 2dF Galaxy Redshift Survey (Verde et al. 2002) suggest that light is essentially unbiased relative to mass on scales larger than 5 Mpc. However, as we discussed earlier in this section, there is some evidence from both observations and simulations (e.g. Benson et al. 2000; Bahcall & Comerford 2002) that light may be biased on smaller scales. A recent study of the *K*-band mass-to-light ratio (Lin, Mohr & Stanford), based on 2MASS luminosities that provide a measure of the stellar mass relatively unaffected by recent star formation history, coupled with mass estimates based on X-ray temperatures, found that M/L_K dropped by a factor ∼2 over the mass range $M(r_{500}) \sim 10^{15}$ to $\sim 10^{14}$ M$_\odot$. Therefore, it may be that the apparent good agreement between our derived galaxy densities and the prediction from the universal mean is fortuitous and that our application of equation (1) leads to an overestimate of r_{500} and hence an underestimate of $\bar{\rho}_{\rm gal}$, which cancels the factor of ∼2–3 by which these densities are biased upwards relative to the Universal mean. Derivation of reliable X-ray masses with *XMM–Newton* may eventually resolve this issue.

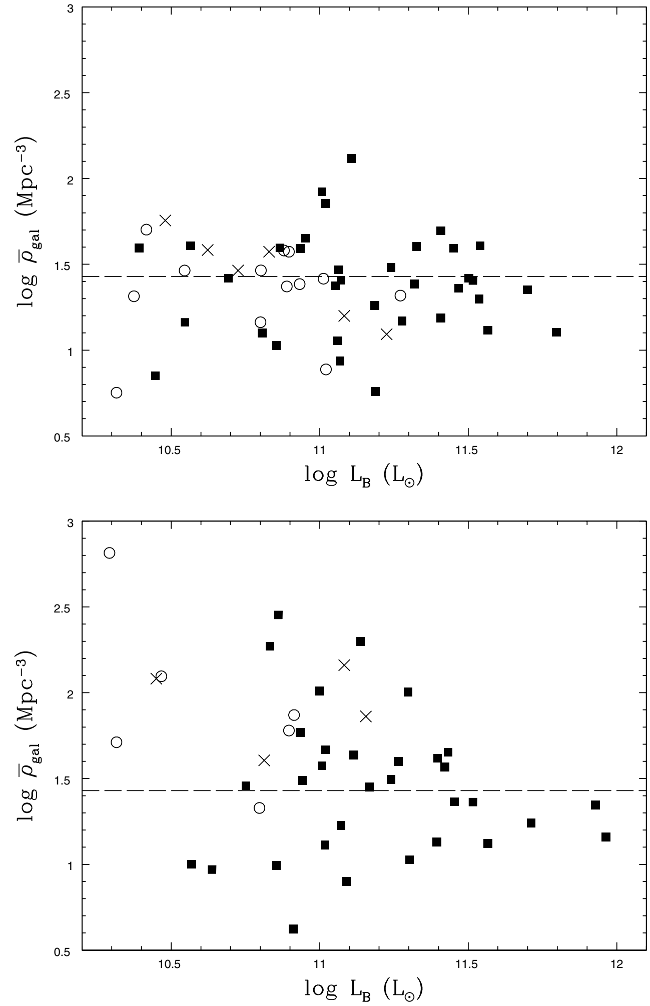

Figure 11. The relationship between $\bar{\rho}_{\rm gal}$ and $L_{\rm B}$ using (top) gas temperature and (bottom) galaxy velocity dispersion, to calculate r_{500} and derive group membership. Filled squares represent the G-sample, open circles the H-sample and crosses non-detections. The expected mean density of galaxies down to our luminosity cut is shown as a horizontal dashed line.

Our conclusion is that the use of equation (1) appears to provide a more stable estimate of r_{500} than the use of a $\sigma_{\rm v}$-based scaling relation, although there is some danger that all our radii may be somewhat overestimated by the $T_{\rm X}^{0.5}$ formula. Where no value of $T_{\rm X}$ is available, we adopt an estimate based on the scaling of scaling of mass with $L_{\rm B}$, using equation (2). In the latter case, an iterative process is involved, because $L_{\rm B}$ depends upon the group membership within r_{500}, whilst r_{500}, in turn, depends on $L_{\rm B}$.

7 GLOBAL SCALING RELATIONS

Scaling relations between the major global parameters of galaxy systems (L_X, T_X, σ_v and L_B) are of great interest in studying the extent to which groups are related to clusters through simple similarity scalings. Previous work (Helsdon & Ponman 2000a,b; Mulchaey 2000; Xue & Wu 2000) has shown that, even where scaling relations follow self-similar forms for rich clusters, this behaviour does not usually extend to the group regime. In terms of X-ray properties, we are interested here in the scaling properties of the hot IGM, so we concentrate primarily on those systems designated as having group emission. In order to compare with cluster properties, we make use of the sample of Horner (2001), based on a homogeneous analysis of data from the *ASCA* observatory. We remove cool ($T_X < 2$ keV), low luminosity ($L_X < 2 \times 10^{43}$ erg s^{-1}) groups from the systems studied by Horner (2001), to give a sample of 230 clusters, 105 of which have velocity dispersions available. The X-ray luminosities for these systems were corrected to r_{200} by Horner (2001), assuming a standard β model with $\beta = 0.67$ and core radius that scales as $L_X^{0.28}$, following the empirical result of Böhringer et al. (2000). We have used the same model to correct each of these cluster luminosities instead to r_{500}, for comparison with our group values. Temperatures for these clusters have been derived by Horner (2001) from MEKAL model fits to integrated *ASCA* spectra from within some extraction radius. Although no attempt was made to remove any emission from a central cool core, we have seen that this has had only a small effect on our own temperatures, so that the two samples can reasonably be compared. Velocity dispersions for a subset of his clusters were collected by Horner (2001) from the literature. Therefore, these will be derived in a heterogeneous fashion. However, for all but three of the clusters, these velocity dispersions are based on more than 10 redshifts.

7.1 The L_X–T_X relation

Strong correlations exist between X-ray luminosity and both gas temperature and velocity dispersion, reflecting the fact that deeper potential wells generally contain more hot gas. It has been clear for many years that the L_X–T_X relation for clusters does not follow the $L_X \propto T_X^2$ law expected for self-similar systems radiating bremsstrahlung X-rays. Most authors (e.g. White, Jones & Forman 1997; Arnaud & Evrard 1999) have found logarithmic slopes close to 3 in the cluster regime, though attempts to remove the effects of central cooling flows (Allen & Fabian 1998; Markevitch 1998) have produced rather flatter relations. Studies of the relation for galaxy groups have mostly found considerably steeper slopes. Helsdon & Ponman (2000a,b) obtained a slope of 4.9 ± 0.8 for a sample of X-ray bright loose groups and 4.3 ± 0.5 for a larger sample (36 systems) including both loose and compact groups. Xue & Wu (2000), found a slope of 5.6 ± 1.8 from data for 38 groups drawn from the literature.

Our result from the GEMS sample, shown in Table 6 and Fig. 12, for the subsample of 45 groups with fitted temperatures, is significantly flatter than the above group results and appears close to the slope seen in clusters. This is especially striking if we restrict our attention to G-sample systems (slope = 2.75 ± 0.46) and flattens still further (2.50 ± 0.42) if we use L_X values extrapolated to r_{500}. In Fig. 13, we plot the G-sample systems, with extrapolated luminosities, alongside the Horner (2001) cluster sample. The parameters for the three trend lines are given in Table 7 and for the G-sample groups is actually somewhat flatter than the cluster relation. Can

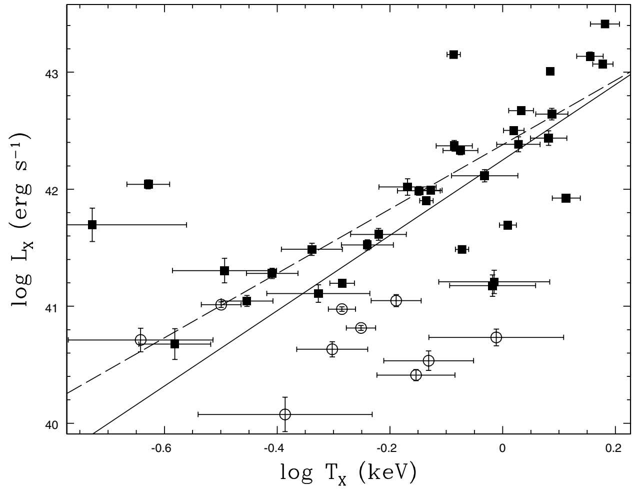

Figure 12. The relationship between L_X and T_X for the GEMS groups. Filled squares represent the G-sample and open circles the H-sample. The solid line represents an unweighted orthogonal regression fit to all points and the dashed line to the G-sample only.

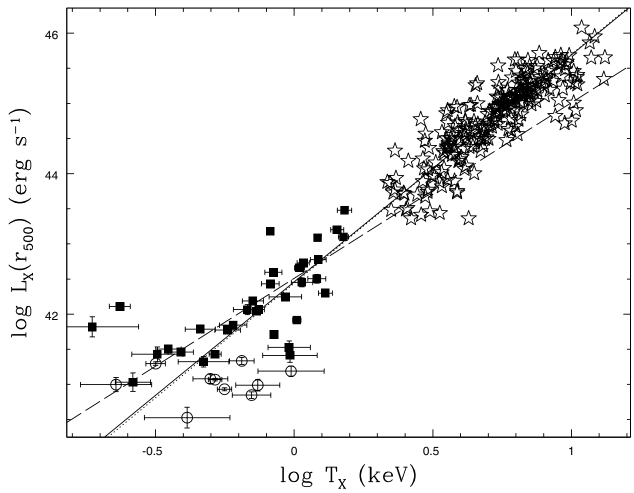

Figure 13. The relationship between $L_X(r_{500})$ and T_X for the GEMS groups (squares and circles) and the Horner clusters (stars). The dashed line represents a fit to the G-sample, the dotted line a fit to the clusters and the solid line a fit to clusters plus the G-sample. The H-sample is excluded from the fitting, but is plotted for comparison.

we conclude from this that the earlier results of a steeper L_X–T_X relation in groups were incorrect?

To explore the origin of the differences from our own earlier results, we examined the subset of 16 of our GEMS groups that overlap with the sample of 24 groups studied by Helsdon & Ponman (2000a). Our regression line through these 16 systems has a slope of 4.3 ± 0.9, close to the result of Helsdon & Ponman (2000a). The use of luminosities extrapolated to r_{500} flattens this regression line only slightly, to a slope of 3.7 ± 1.0. These tests strongly suggest that the flatter slope from our G-sample systems is primarily related to differences in the group sample used here, rather than in the analysis techniques employed. The systems studied by Helsdon & Ponman (2000a) were selected on the basis of significant X-ray flux and therefore constitute a sample of X-ray bright groups, whereas the GEMS sample was deliberately designed to cover a

Table 7. A comparison of scaling relations between groups and clusters. Group relations are derived from the G-sample and cluster relations from the sample of Horner (2001).

Relation		Groups		Clusters		All		Figure
		Slope	Intercept	Slope	Intercept	Slope	Intercept	
$\log L_X(r_{500})$	$\log T_X$	2.50 ± 0.42	42.51 ± 0.09	3.26 ± 0.12	42.44 ± 0.10	3.23 ± 0.10	42.46 ± 0.07	13
$\log L_X(r_{500})$	$\log \sigma_v$	2.31 ± 0.61	36.53 ± 1.54	3.94 ± 0.33	33.24 ± 0.97	4.55 ± 0.25	31.34 ± 0.72	15
$\log \sigma_v$	$\log T_X$	1.15 ± 0.26	2.60 ± 0.03	0.78 ± 0.05	2.36 ± 0.04	0.71 ± 0.05	2.43 ± 0.03	16

wider spectrum of X-ray properties, as discussed in Section 2. As a result, our present sample includes a much larger number of cool groups ($T_X < 0.7$ keV) than that of Helsdon & Ponman (2000a) and most other previous studies. Two groups in particular, HCG 10 and NGC 3557, have $T_X < 0.25$ keV and yet have moderately high X-ray luminosities.

In the present study, we are also pushing closer to the statistical limits of what can be achieved with *ROSAT* data. It is well established that there is considerably larger real scatter in the scaling relations for galaxy groups than is seen in clusters. This scatter introduces three sources of bias into our regression process. First, the result of truncating this scattered trend at low L_X (because we will either reject systems with very low L_X as galaxy halo sources, or fail to detect them altogether) will be to flatten the fitted relation. Secondly, there is a logarithmic bias whereby the scatter in $\log T_X$ (which dominates the statistical scatter about the trend line) will be asymmetric (if the scatter in T_X is fairly symmetric) with larger scatter towards low $\log T_X$. Because the statistical errors are largest in systems with lowest L_X, this will also tend to flatten the regression line. Thirdly, there is an additional bias that couples with the scatter in T_X. At temperatures towards the bottom of the *ROSAT* bandpass and close to the absorption cut-off resulting from interstellar gas and dust, the unabsorbed bolometric flux corresponding to a given PSPC count rate rises quite sharply as T_X falls (e.g. for an absorbing column of 4×10^{20} cm^{-2} it rises by 67 per cent as T_X falls from 0.6 to 0.3 keV). Thus, it follows that points in the L_X–T_X plane that scatter down in temperature will also scatter up in L_X, which further magnifies the flattening effect discussed above. Because all three of these biases are related to the large scatter in the data, we investigated the effect of clipping the outliers. Iteratively discarding G-sample points that lie more than 2σ from the regression line does indeed steepen the fitted slope, from 2.5 to 3.0 where 8 of the 33 points are clipped in this analysis. Note, however, that this steeper slope is still fully consistent with the cluster L_X–T_X relation.

One final source of bias, which becomes important when pushing the sample down to very poor groups, is the impact of contamination from point sources that are unresolved by *ROSAT*. Because the fractional contribution of such sources will tend to be larger in the lowest luminosity groups, it will tend to flatten the L_X–T_X relation. Helsdon, Ponman & Mulchaey (2004) find, from a comparison of *Chandra* and *ROSAT* results for two very cool groups, that the level of unresolved point-source contribution to the diffuse flux derived from the PSPC analysis is 30–40 per cent. So this effect is smaller than the correction (a factor 2–3 for such poor systems) arising from extrapolation to r_{500} and works in the opposite direction.

A further difference in our present analysis, compared to earlier studies, is that we separate off systems in which the X-ray emission appears to be related to a central galaxy, rather than to the group as a whole. In studying the properties of groups, for comparison with clusters, this seems the appropriate thing to do. As can be seen from Fig. 12 and Table 6, these halo sources do fall at the bottom of the L_X–T_X plot and their inclusion steepens the fitted L_X–T_X relation. However, this will have had little impact on the earlier work of Helsdon & Ponman (2000a), because their X-ray bright sample contained very few objects that might be classified as galaxy halo sources.

In summary, we conclude that although the L_X–T_X relation obtained from our G-sample groups is close to continuous with the cluster relation, albeit with increased scatter, this may be a misleading result because we have identified a number of biases, all of which work towards flattening the fitted L_X–T_X relation in the low-T_X, low-L_X regime. Extension of the data towards lower L_X would be necessary to reduce these biases and establish definitively whether the L_X–T_X relation does steepen in groups. This may ultimately be possible with *XMM–Newton*, but will not be straightforward, in a regime where luminosities are comparable to those of individual haloes around early-type group member galaxies. What is clear from our results, is that groups show a considerably larger real scatter about the mean L_X–T_X trend than is seen in clusters: spanning at least a factor of 30 in L_X, at a given value of T_X, or a factor 3–4 in T_X at a given L_X.

7.2 L_X–σ_v relation

Our relationship between L_X and σ_v (Fig. 14) has a slope of 2.56 $\pm$ 0.56 for the G-sample, which is flatter than the value of 4.5 $\pm$ 1.1 found by Helsdon & Ponman (2000a). Although there is general agreement that the L_X–σ_v relation does not steepen in groups, unlike the L_X–T_X relation, there is disagreement between studies (e.g Ponman et al. 1996; Mulchaey & Zabludoff 1998; Helsdon & Ponman 2000a; Mahdavi 2001), which find that groups are consistent with the cluster-relation slope of ≈4, and those (Mahdavi

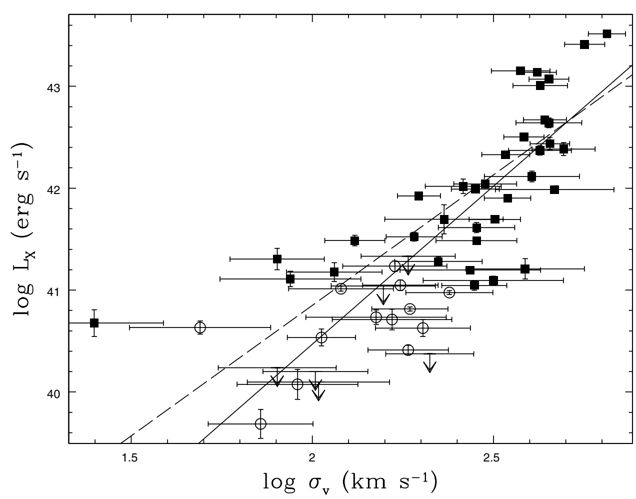

Figure 14. The relationship between L_X and σ_v for the GEMS groups. Filled squares represent the G-sample, open circles the H-sample and arrows represent upper-limits from non-detections. The solid line represents an unweighted orthogonal regression fit to all points and the dashed line to the G-sample only.

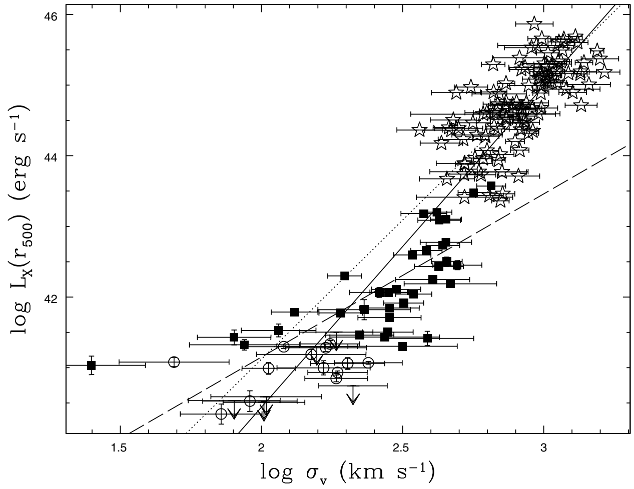

Figure 15. The relationship between $L_X(r_{500})$ and σ_v for the GEMS groups (squares, circles and arrows) and the Horner clusters (stars). The dashed line represents a fit to the G-sample, dotted line to the clusters and solid line to clusters plus the G-sample. The H-sample and non-detections are excluded from the fitting but are plotted for comparison.

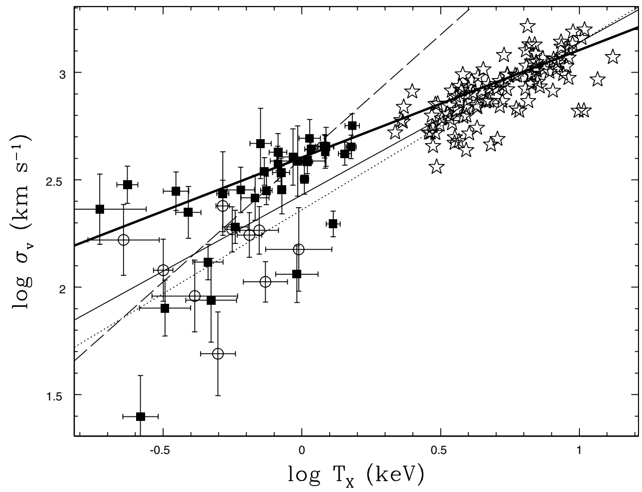

Figure 16. The relationship between σ_v and T_X for the GEMS groups (squares and circles) and the Horner clusters (stars). The dashed line represents a fit to the G-sample, dotted line to the clusters and solid line to clusters plus the G-sample. The H-sample is excluded from the fitting but is plotted for comparison and the bold line represents $\beta_{spec} = 1$.

et al. 1997; Helsdon & Ponman 2000b; Mahdavi et al. 2000; Xue & Wu 2000), which find significantly flatter relations in groups. The result from the GEMS sample is clearly (Fig. 15) substantially flatter than the cluster trend and has a slope in good agreement with that of Helsdon & Ponman (2000b) (2.4 ± 0.4) and Xue & Wu (2000) (2.35 ± 0.21). Extrapolation of the luminosity to r_{500} results, as expected, in a slightly lower slope of 2.31 ± 0.62 (Table 7).

As with the L_X–T_X relation, biases are at work that will tend to lead to some spurious flattening of our regression results. Because the groups with lowest L_X tend to be the poorest and hence to have the largest fractional errors in σ_v, three of the four sources of bias discussed in the last section (the truncation and logarithmic biases and point-source contamination) will also apply to the L_X–σ_v relation. None the less, there are some groups in our sample with remarkably low-velocity dispersion, which appear to show group-scale emission. This is hard to understand, since such X-ray emission presumably implies that a group is collapsed, if not virialized, and as Mamon (1994) has argued, the requirement that collapsed systems should have some minimum overdensity sets a lower bound (at a given mass or radius) to the velocity dispersion which they can have. This bound is ∼100–200 km s^{-1} for poor groups. A study with *Chandra* (Helsdon et al. 2004), of two of the low-σ_v systems in our sample, NGC 1587 and NGC 3665, has confirmed that the diffuse X-ray emission identified by *ROSAT* is not grossly misleading, although point-source contamination and inaccurate spectral characterization can lead to overestimation of L_X by ∼30–40 per cent.

The fact that groups with such low values of σ_v can contain a significant IGM, with properties which accord reasonably with those of other groups, strongly suggests that the observed values of σ_v are not reflecting the depth of the potential well in the way one expects. We will return to this in the following section.

7.3 σ_v–T_X and β_{spec}

A number of previous studies have found that the relationship between velocity dispersion and gas temperature departs slightly from the virial theorem expectation ($\sigma_v \propto T_X^{0.5}$) in clusters (Bird, Mushotzky & Metzler 1995; Girardi et al. 1998; Wu, Xue & Fang 1999). The evidence for groups is more controversial, with some authors (e.g. Mulchaey 2000; Xue & Wu 2000) finding that groups fall on the cluster trend and others (Helsdon & Ponman 2000a,b) finding that the relation steepens in groups with $T_X < 1$ keV, to a slope $\geqslant$1. Our result, presented in Fig. 16, shows that there is a great deal of non-statistical scatter in the groups, in addition to the large statistical errors in both T_X and especially σ_v, in the poorest systems. This appears to be the origin of the controversy over whether the relation does or does not steepen in the group regime. Formally, we find that it does, with a best-fitting slope to the GEMS G-sample systems of 1.15 ± 0.29. However, it is clear that the best-fitting line to the combined group + cluster sample (with a slope of 0.71 ± 0.05) passes through the centre of the scatter of group points and also represents the trend in the cluster regime quite adequately. This slope is somewhat steeper than that found in most previous studies.

Comparison with the line $\beta_{spec} = 1$ in Fig. 16, shows that many of the G-sample groups are actually consistent with this energy equipartition line (as are many clusters), but that there is a significant subsample of points that scatter well below it. These systems have velocity dispersions typically a factor 3 below what would be expected for their X-ray temperatures. All of the groups with $\sigma_v \lesssim$ 100 km s^{-1} fall into this category.

Fig. 17 shows clearly that high X-ray luminosity ($L_X > 10^{42}$ erg s^{-1}) groups have $\beta_{spec} \sim 1$, whilst groups with $L_X \lesssim 10^{41.5}$ erg s^{-1} scatter widely in β_{spec}, spanning the range $\beta_{spec} = 0.1$–1.0. The evidence discussed in Section 6 above led us to the conclusion that T_X gives a much more reliable measure of system mass and radius than does σ_v. It follows from this that the problem in some of the poorest systems, which leads to their remarkably low values of β_{spec}, lies not with T_X, but with σ_v. Some of these groups, from both G- and H-samples, have extremely low-velocity dispersions, giving them low β_{spec}, and also small radii (and hence high $\bar{\rho}_{gal}$) when these are calculated on the basis of σ_v.

As can be seen from Table 2, most of these low-σ_v systems have $\leqslant$ 6 galaxy redshifts available for the computation of σ_v. Under these circumstances, a number of biases may affect the derived value of σ_v

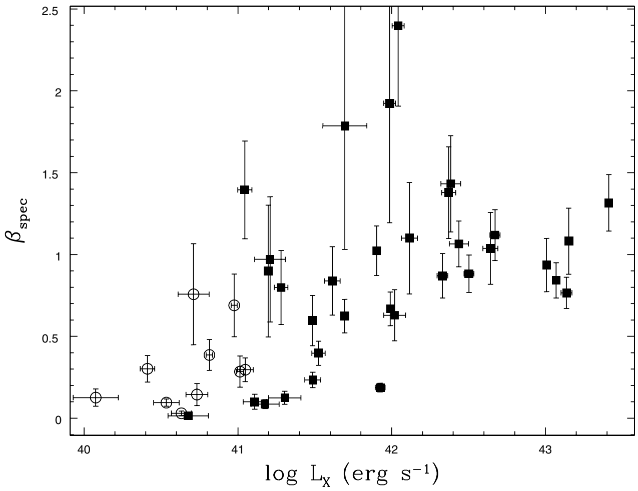

Figure 17. The relationship between $\beta_{\rm spec}$ and $L_{\rm X}$. Filled squares represent the G-sample and open circles the H-sample.

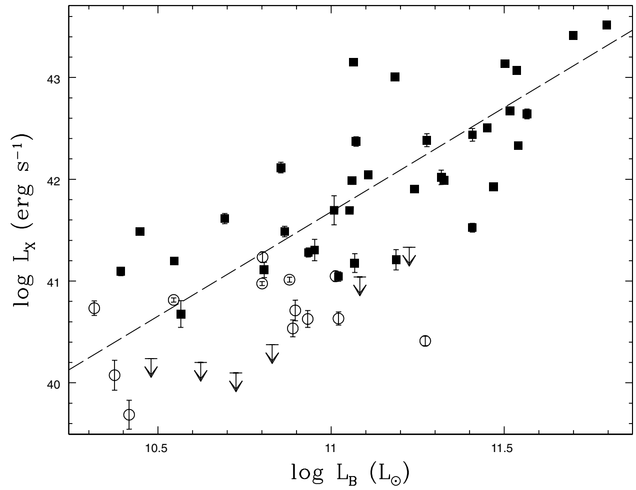

Figure 18. The relationship between $L_{\rm X}$ and $L_{\rm B}$. Filled squares represent the G-sample, open circles the H-sample and arrows represent upper-limits from non-detections. The dashed line represents a fit to the G-sample.

(Helsdon & Ponman, in preparation). We have already corrected for a statistical bias that results if one uses the normal unbiased estimator for $\sigma_{\rm v}^2$ and then takes the square root to obtain $\sigma_{\rm v}$ (which is then not unbiased). This is the origin of the term 3/2 (rather than 1) in the denominator of equation (4). However, another downward bias may arise if (as is normally the case for X-ray bright groups) one of the galaxies is at rest at the bottom of the group potential well. This galaxy will not contribute to the sum of squared deviations from the mean velocity, but will be included in the denominator. For a group with only four members, this reduces $\sigma_{\rm v}$ by over 20 per cent. However, such statistical biases cannot provide anything approaching the large factors ($\sim$2–3) by which we infer that $\sigma_{\rm v}$ has been reduced in some of these groups.

Physical effects that might lead to such low values of $\sigma_{\rm v}$, are discussed in greater detail in Helsdon et al. (2004). Observed galaxy velocity dispersions might be reduced if: (i) galaxy orbits decay as a result of dynamical friction, (ii) orbital energy is converted into internal energy of galaxies via tidal heating, or (iii) orientation effects result in most of the galaxy velocity vectors for some systems lying close to the plane of the sky. The last of these has, perhaps, the greatest potential to achieve really substantial reductions in observed line-of-sight velocity dispersions.

7.4 Scaling between $L_{\rm B}$ and X-ray properties

In an ensemble of self-similar groups with constant mean density, the X-ray luminosity would scale linearly with galaxy mass and hence with optical luminosity. Helsdon & Ponman (2003b) found a much steeper relation, $L_{\rm X} \propto L_{\rm B}^{2.69\pm0.29}$. Our fitted relation for our full sample of X-ray detected systems is consistent with this (Table 6). The trend for the G-sample systems (Fig. 18) is somewhat flatter (2.05 $\pm$ 0.21), but still much steeper than the self-similar expectation. This could be explained in any of three ways:

(i) $f_{\rm gas}$ rises with system mass,
(ii) gas density is higher in more massive systems,
(iii) star formation is more efficient in poorer groups.

There are indications that all three of these factors may contribute, but the results of Ponman et al. (1999) and Sanderson et al. (2003) suggest that the dominant effect is probably a reduction in gas density in the inner regions of poor systems, relative to richer ones.

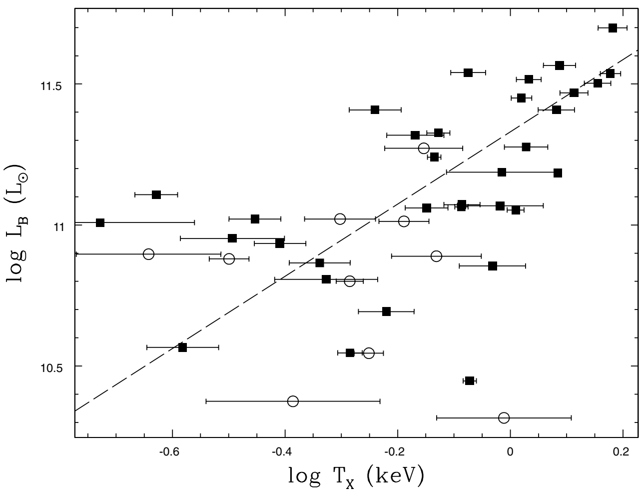

Figure 19. The relationship between $L_{\rm B}$ and $T_{\rm X}$. Filled squares represent the G-sample and open circles the H-sample. The dashed line represents a fit to the G-sample.

If $T_{\rm X}$ gives a reliable measure of group size ($R \propto T_{\rm X}^{0.5}$) and hence mass, as we are assuming here (because we use this relation to define our value of r_{500}), then $L_{\rm B} \propto T_{\rm X}^{1.5}$ would result if SFE were independent of system mass. Our observed relation (Fig. 19) has a slope 1.28 $\pm$ 0.19, somewhat flatter than the slope of 1.64 $\pm$ 0.23 found by Helsdon & Ponman (2003b), but still consistent with the value of 1.5 expected from self-similarity and constant SFE. If, however, the $M{-}T_{\rm X}$ relation has a slope steeper than the value of 1.5 (i.e. $M \propto T_{\rm X}^{1.5}$) as has been found by a number of previous studies [e.g. Nevalainen et al. (2000), Finoguenov et al. (2001) and Sanderson et al. (2003) suggest a slope $\approx$1.8], then our $L_{\rm B}{-}T_{\rm X}$ slope of 1.28 suggests an SFE that is significantly higher in lower mass systems, as discussed in Section 6.

8 β AND THE ROLE OF HEATING

Mulchaey & Zabludoff (1998) and Helsdon & Ponman (2000a) found that most X-ray bright groups with data of sufficiently high quality require two-component β models to adequately represent their surface brightness distributions. The central component is identified either with a halo associated with the brightest cluster galaxy (BCG) (Mulchaey & Zabludoff 1998), or a central group cooling region (Helsdon & Ponman), whilst the outer component clearly arises from a group-scale intergalactic medium. Helsdon & Ponman (2000a) investigated the effect of fitting a single-component β model to a group where a two-component model is more appropriate and found that the value of $\beta_{\rm fit}$ obtained with a single-component model typically scattered by $\sim$0.1 (but *in extremis* by up to 0.3), either upward or downward from the value for the group component given by a two-component fit. We therefore place more credibility in the two-component results from our present fits.

The largest value of $\beta_{\rm fit}$ obtained for any of the GEMS groups is 0.58 and the median value from our G-sample fits is 0.45, in good agreement with the value of 0.46 derived by Helsdon & Ponman (2000a). This is clearly well below the typical value, $\beta_{\rm fit} \approx 0.67$, found in rich clusters (Arnaud & Evrard 1999; Mohr, Mathiesen & Evrard 1999). A trend towards lower values of $\beta_{\rm fit}$ in poorer clusters has been reported by a number of authors. However, Mohr et al. (1999) found that this trend disappeared when the systems in their study (which all had $T_{\rm X} \gtrsim 2$ keV) were fitted with two-component models and hence concluded that the effect was spurious. This explanation can account for neither the low values of $\beta_{\rm fit}$ obtained here, nor those found in the studies of Helsdon & Ponman (2000a) or MDMB, because two-component fits are employed wherever possible and are found to give $\beta_{\rm fit} \sim 0.4$–0.5.

However, some uncertainty arises as a result of the fact that X-ray emission in groups can typically be traced only to a modest fraction of the radii to which they should be virialized (Mulchaey 2000). It has been argued on the basis of simulations (Navarro, Frenk & White 1995) and analytical models (Wu & Xue 2002) that gas density profiles steepen progressively and hence that low values of $\beta_{\rm fit}$ naturally arise when profiles are fitted only within $r \sim 0.3\, r_{200}$. However, there is some evidence that this is unlikely to explain the low values of $\beta_{\rm fit}$ we observe. Sanderson et al. (2003) examined the effects of truncating the data for galaxy clusters when fitting β models and found little evidence for any significant drop in $\beta_{\rm fit}$. Moreover, observed radial surface brightness profiles are generally found to be modelled remarkably well by simple power laws, outside the central core. Vikhlinin, Forman & Jones 1999 studied a sample of rich clusters out to $r \sim r_{200}$ with the *ROSAT* PSPC and found only a slight steepening (by $\Delta\beta \approx 0.05$) in the outer regions of typical clusters. Rasmussen & Ponman (2004) were able to trace the emission from two rich groups ($T_{\rm X} \sim 2$ keV) out to r_{500} and found no evidence for steepening of the profiles beyond the simple β-model fits.

Whilst the $\beta_{\rm fit}$ values of groups appear to be lower than those of clusters, no previous studies have detected any significant correlation between $\beta_{\rm fit}$ and $T_{\rm X}$ within the group regime. Fig. 20 shows the relationship between these two variables for the GEMS groups. Results from two-component fits are marked as larger symbols. No correlation is apparent for the G-sample systems: in fact, a weak (1.4σ) anticorrelation is present in these data. The results for groups with two-component fits (i.e. the most reliable values) show no significant trend at all.

It is interesting to compare the values of $\beta_{\rm fit}$ and $\beta_{\rm spec}$ for the GEMS groups, and this is plotted in Fig. 21. In the simple case of an isothermal hot gas and a set of galaxies with isotropic velocity dispersion, both in equilibrium in the gravitational potential of a mass distribution having the β-model form, one would expect to find $\beta_{\rm fit} = \beta_{\rm spec}$. Even though the assumptions underlying this model are restrictive and unrealistic, one might in general expect to find a correlation between the two β if heating of the IGM is affecting the gas density profiles, as is often assumed (Balogh, Babul & Patton 1999; Cavaliere, Menci & Tozzi 1999), because energy input into the gas is expected to directly reduce $\beta_{\rm spec}$ and also to flatten the gas profile, lowering $\beta_{\rm fit}$ (cf. Muanwong et al. 2002). In practice, no such relationship is seen. $\beta_{\rm spec}$ covers a much wider range than $\beta_{\rm fit}$, with many systems having $\beta_{\rm spec} \sim 1$ and some having extremely low values $\beta_{\rm spec} \sim 0.1$. However, the latter do not have remarkably low values of $\beta_{\rm fit}$.

How can we understand the lack of significant correlations involving $\beta_{\rm fit}$? If group mass, coupled to a simple universal pre-heating model, were responsible for the flatter profiles in groups compared to clusters, then strong correlations would be seen. Hence, one plausible suggestion is that additional properties peculiar to individual groups, such as SFE or merger history, play a substantial role and introduce a large amount of non-statistical scatter. Flat X-ray surface

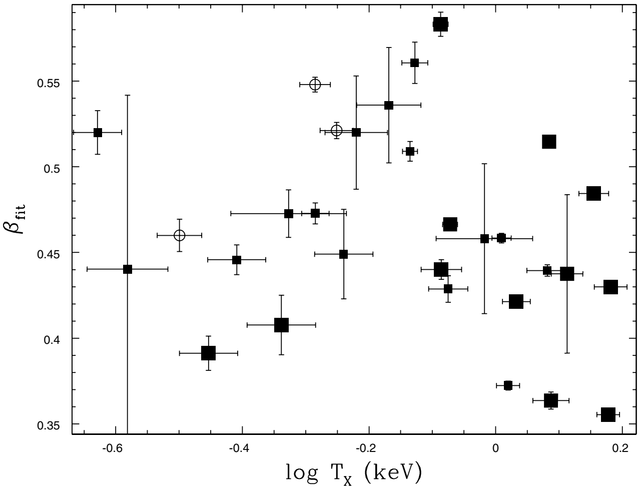

Figure 20. The relationship between $\beta_{\rm fit}$ and $T_{\rm X}$. Filled squares represent the G-sample and open circles the H-sample. Larger points denote systems in which a two-component β model was fitted.

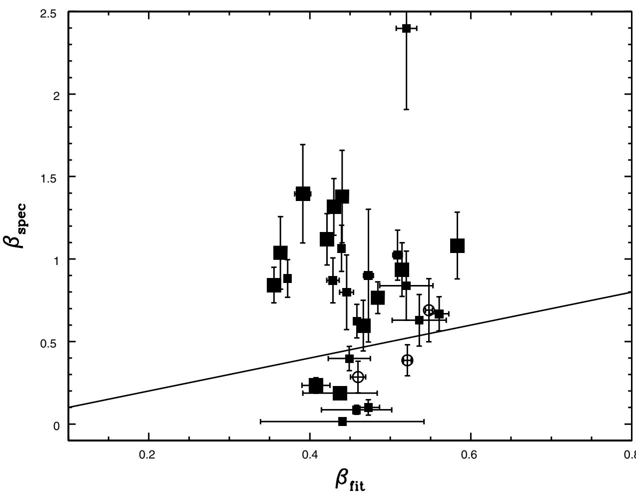

Figure 21. The relationship between $\beta_{\rm spec}$ and $\beta_{\rm fit}$. Filled squares represent the G-sample and open circles the H-sample. Larger points denote systems in which a two-component β model was fitted and the solid line represents equality.

brightness profiles are associated with lower central gas densities and consequently with higher entropy compared with self-similar expectations. Recent results (Mushotzky 2003; Ponman, Sanderson & Finoguenov 2003; Pratt & Arnaud 2003; Sun et al. 2003) suggest that the earlier hypothesis (Ponman et al. 1999) of a universal-floor value of entropy was incorrect. It appears (Ponman et al. 1999) that entropy scales in a non-self-similar way with system mass and that there is also significant scatter (Mushotzky 2003; Sun et al. 2003) between the magnitude of the entropy in groups of a given mean temperature. This would lead to scatter in the value of $\beta_{\rm fit}$, making it hard to detect any trend with temperature without a large and accurately modelled sample. Because biases are present where only one-component fits are performed, we actually have only 15 reliable values of $\beta_{\rm fit}$ in our sample.

The lack of correlation between $\beta_{\rm fit}$ and $\beta_{\rm spec}$, is not obviously explained by this explanation of individual scatter. What is required is some way of breaking the link between the two β values. The obvious way to do this is through effects on $\sigma_{\rm v}$, because the expectation that the two β should be related, is based on the assumption that $\sigma_{\rm v}$ provides a measure of the gravitational potential. We have already seen, from the discussion in Sections 6 and 7.3, that there is good reason to doubt this assumption.

9 GALAXY MORPHOLOGY

9.1 Spiral fraction in groups

Strong correlations between $f_{\rm sp}$ and both $L_{\rm X}$ and $T_{\rm X}$ are seen in clusters (Edge & Stewart 1991a). In groups, such trends have proved to be surprisingly weak (Ponman et al. 1996; Mulchaey 2000; Helsdon & Ponman 2003b), despite the strong correlation between X-ray emission and the morphology of the central group galaxy (discussed below). For the G-sample systems, we also find only a weak (1σ) tendency for $f_{\rm sp}$ to be higher in low-$L_{\rm X}$ groups, but the correlations of $f_{\rm sp}$ with $T_{\rm X}$ and $\sigma_{\rm v}$ (see Table 6) are stronger, though they still show a large amount of scatter (Figs 22 and 23). This is consistent with what Ponman et al. (1996) found in their study of Hickson compact groups. Because $T_{\rm X}$ and $\sigma_{\rm v}$ are primarily determined by the depth of the potential well, whilst $L_{\rm X}$ is related to the mass and density of hot gas, the relative strengths of these correlations, now found for both loose and compact groups, is that galaxy morphology is related to the depth of the potential rather than its gas content.

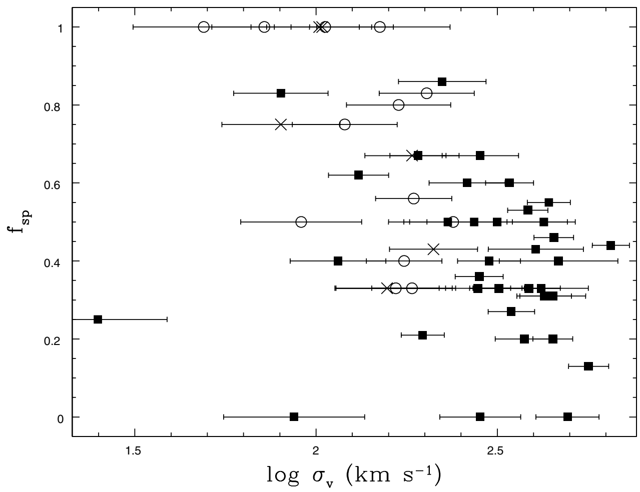

Figure 23. The relationship between $f_{\rm sp}$ and $\sigma_{\rm v}$. Filled squares represent the G-sample, open circles the H-sample and crosses non-detections.

Comparing the $f_{\rm sp}-T_{\rm X}$ correlation with that seen in clusters (Edge & Stewart 1991b), there is a large offset between the two relations. The cluster relation shows $f_{\rm sp}$ rising from ∼0.1 in hot clusters like Coma, to ∼0.5 in systems like Virgo, with $T_{\rm X}$ = 2–3 keV. In contrast, a best-fitting trend through the G-sample $f_{\rm sp}-T_{\rm X}$ data, is fitted by $f_{\rm sp} = 0.26–0.93 \log T_{\rm X}$, corresponding to a typically low value of $f_{\rm sp}$ for groups with $T_{\rm X} > 1$ keV. Proper comparison of the group and cluster samples requires the application of consistent absolute magnitude limits to all systems and lies beyond the scope of the present paper, but would be very worthwhile.

Although the relationship between $f_{\rm sp}$ and $L_{\rm X}$ is not strong within the G-sample, when the full sample is considered, it becomes a great deal stronger (3.5σ), as shown in Fig. 24. It is clear that galaxy halo sources and X-ray undetected sources (which of course have lower $L_{\rm X}$ than most G-sample groups) tend to have systematically higher $f_{\rm sp}$ than do X-ray bright groups. It seems that the presence of detectable hot intergalactic gas is related to galaxy morphology much more strongly that its luminosity.

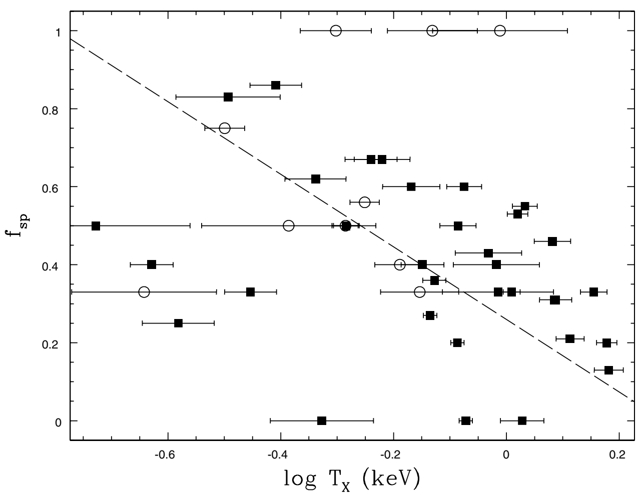

Figure 22. The relationship between $f_{\rm sp}$ and $T_{\rm X}$. Filled squares represent the G-sample and open circles the H-sample. The dashed line represents a fit to the G-sample.

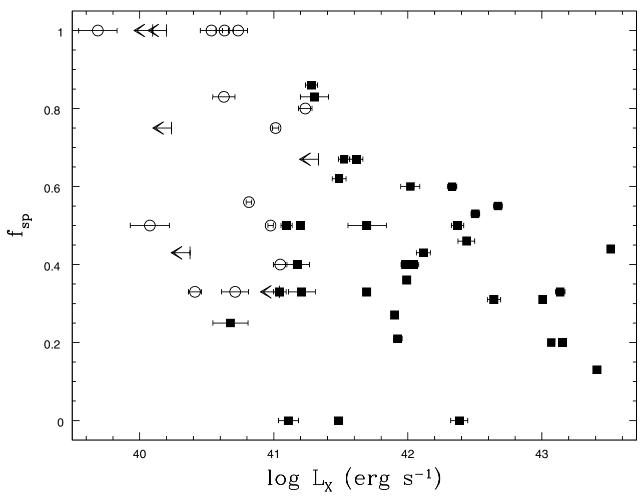

Figure 24. The relationship between $f_{\rm sp}$ and $L_{\rm X}$. Filled squares represent the G-sample, open circles the H-sample and arrows represent upper-limits from non-detections.

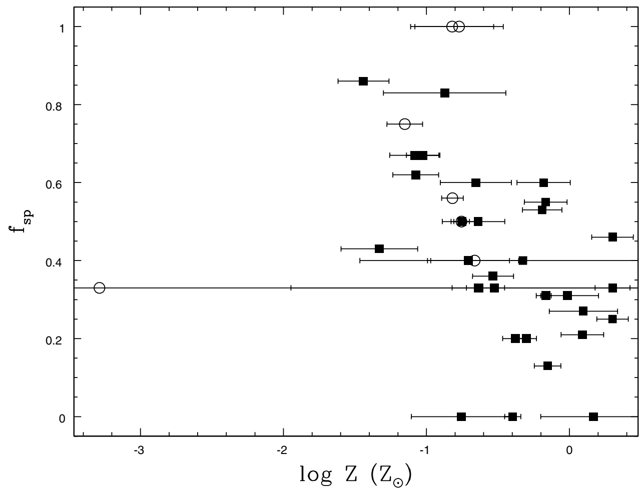

Figure 25. The relationship between $f_{\rm sp}$ and Z. Filled squares represent the G-sample and open circles the H-sample.

In general, metallicities derived from *ROSAT* PSPC spectra must be regarded with considerable caution, because the spectral resolution of the instrument is very limited and it is well known that serious biases can result if multitemperature gas is fitted with a single-temperature hot plasma model (Buote & Fabian 1998). None the less, the 3σ anticorrelation between metallicity and spiral fraction (Fig. 25) is sufficiently strong to be worthy of comment. Taken at face value, this would seem to imply that most of the intergalactic metals have their origin in early-type galaxies. Such a result can be understood if the formation of early-type galaxies, either by galaxy merging or through some primordial collapse (or more likely early-epoch multiple merging) picture, results in the ejection of much of the enriched interstellar medium of the galaxy as a result of energy input from Type II supernovae (Matteucci & Tornambe 1987; Kauffmann & Charlot 1998). However, the role of biases in *ROSAT* metallicity estimates is potentially sufficiently serious that this result requires careful checking with CCD quality spectra. This is underway at present.

Finally, in Fig. 26, we show the relationship between spiral fraction and mean galaxy density. It was shown by Helsdon & Ponman (2003a) that groups display a morphology–density relation rather similar to clusters, in the sense that galaxies in regions of high surface density are more likely to be of early type. Here we see the opposite effect, in terms of the mean density of groups as a whole: there is a tendency, with a great deal of scatter, but significant at the 2.5σ level (Table 6), for groups with the highest mean density to have higher $f_{\rm sp}$. This is not necessarily in conflict with the Helsdon & Ponman (2003a) result, which was a local effect. If all these groups had virialized recently, we would actually expect them all to show the same mean density (as discussed in Section 6 above), so that no correlation at all would be expected between $f_{\rm sp}$ and $\bar{\rho}_{\rm gal}$, even if a local morphology–density relation were present. The fact that we see a systematic trend suggests that the range of values of $\bar{\rho}_{\rm gal}$ that we observe (which span a factor of $\sim$30) is not simply the result of statistical scatter, but is subject to some systematic effects, which are related to the morphological mix in groups. For example, most of the groups with mean densities significantly higher than the expected value (marked in the figure) have reasonably high values of $f_{\rm sp}$. This could result from underestimation of their r_{500} values, which are based on gas temperatures for most groups. One explanation could be that these groups are not fully virialized, so that their gas temperature has yet to rise to its final value.

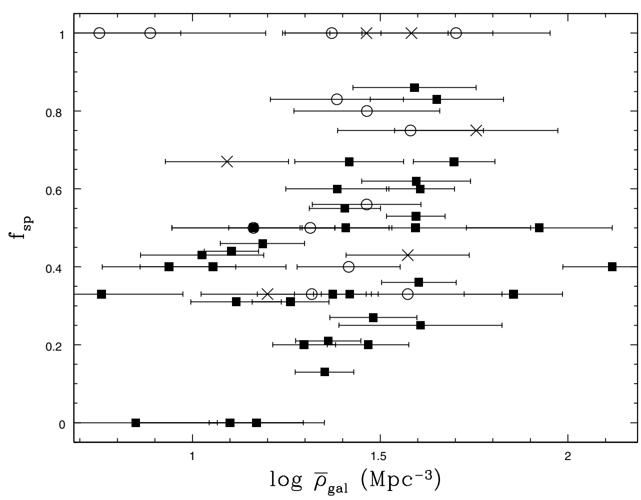

Figure 26. The relationship between $f_{\rm sp}$ and $\bar{\rho}_{\rm gal}$. Filled squares represent the G-sample, open circles the H-sample and crosses non-detections.

9.2 Brightest group galaxies

The most striking correlation between the X-ray properties of groups and their galaxy contents, which has been noted since early *ROSAT* studies of groups (Ebeling, Voges & Boehringer 1994), is the presence of a bright early-type galaxy at the centre of the X-ray emission in virtually every X-ray bright group. This phenomenon is clearly apparent in the GEMS sample, as can be seen from Fig. 27. Of our 35 G-sample systems, 32 have an early-type BGG and in all but four of these, this galaxy lies at the centre of the X-ray halo of the group. As described in Section 3, we have defined our BGG to be the most optically luminous within $0.25r_{500}$ of the group centre, in order to avoid picking up outlying galaxies that may have recently fallen into a group. With this definition, we find that all but three of the systems with group-scale emission (hatched regions) have early-type BGGs. These three exceptions are HCG 16, 48 and 92. HCG 16 is well known as an unusual group dominated by spirals that shows significant intergalactic hot gas (Ponman et al. 1996; Dos

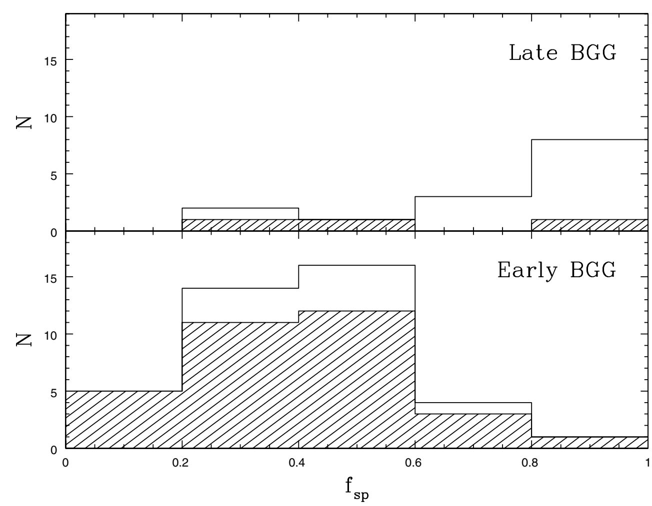

Figure 27. A histogram showing the distribution of $f_{\rm sp}$ for systems dominated by a late-type galaxy and those dominated by an early-type galaxy. The shaded region represents the G-sample.

Santos & Mamon 1999) and probably corresponds to a system that is collapsed but not yet virialized (Belsole et al. 2003). HCG 92 is the well studied system Stephan's Quintet, which contains a number of strongly interacting galaxies. None of the member galaxies lies at the centre of the X-ray emission and high-resolution observations (Pietsch et al. 1997; Sulentic et al. 2001) have shown sharp features in the X-ray emission, interpreted as intergalactic shocks. Like HCG 16, this appears to be a newly collapsed group. Finally, in HCG 48 the late-type BGG does appear to lie at the centre of the diffuse X-ray emission, although a bright elliptical is seen 71 kpc away in projection. The unusual properties of this group may be related to the fact that it appears to be falling into the nearby cluster Abell 1060 and its X-ray morphology is distorted into a coma-like shape.

The distribution of spiral fraction in detected and undetected groups can be seen from Fig. 27 to differ primarily in that there is a set of groups with high $f_{\rm sp}$ and late-type BGGs, which almost invariably show no group-scale X-ray emission. It can be seen from Fig. 28 that these systems (and indeed all groups without detectable group-scale hot gas) also have low-velocity dispersions. It seems very likely that these systems are not yet fully collapsed and virialized, so that their IGM has not been heated and compressed to a point where it radiates detectable X-rays. Note, however (e.g. from Fig. 11), that these H- and U-sample systems do not generally have low inferred mean densities. This is not entirely surprising, because they have been selected from group catalogues that are compiled using techniques that rely on a significant overdensity in the inferred three-dimensional density, typically corresponding, for the catalogues we draw from, to a threshold factor of ∼20–80, relative to the mean density of the Universe: although all our systems appear to lie well above this threshold.

Fig. 29 shows a highly significant (6σ, including all points in the plot) tendency for brighter BGGs to be found in richer groups (i.e. with higher total $L_{\rm B}$). A similar, but less significant (2.5σ) correlation exists between $L_{\rm BGG}$ and $L_{\rm X}$. These relationships are similar in character to those seen in the BCGs, found in richer systems, and represent an extension towards poorer systems of the trends with X-ray luminosity and temperature reported by Edge (1991). Studies of the K-band luminosities of BCGs (Burke, Collins & Mann 2000; Brough et al. 2002) in clusters spanning a range of redshifts and X-ray luminosities, show a correlation between $L_{\rm X}$ and $L_{\rm BGG}$, although Brough et al. (2002) argue that this relation is weak in low-redshift ($z < 0.1$) clusters. Ours is a low-redshift sample and yet clearly does show such a correlation. This is in accord with the results of Burke et al. (2000), who found BCGs in the most X-ray luminous clusters to be standard candles, whilst for poor clusters ($L_{\rm X} < 10^{44}$ erg s^{-1} in our cosmology) they find that lower luminosity clusters tend to contain less bright BCGs. Our results show that this trend continues through the group regime.

It seems very likely (Dubinski 1998) that BCGs and BGGs are primarily assembled through galaxy merging. This idea is also supported, from the present study, by the fact that early-type BGGs tend to be more luminous (on average by a factor 1.8) than late-type BGGs. Because (other things being equal) the merger rate should be higher in systems with low-velocity dispersion, it is of some interest to examine the relationship between $L_{\rm BGG}$ and $\sigma_{\rm v}$. This is shown in Fig. 30 and shows a tendency (1.9σ) towards brighter BGGs in higher velocity dispersion systems. There is a strong clue here, that much of the merging involving the galaxies that we now see in the more luminous groups must have happened at earlier epochs. We will return to this in Section 10.

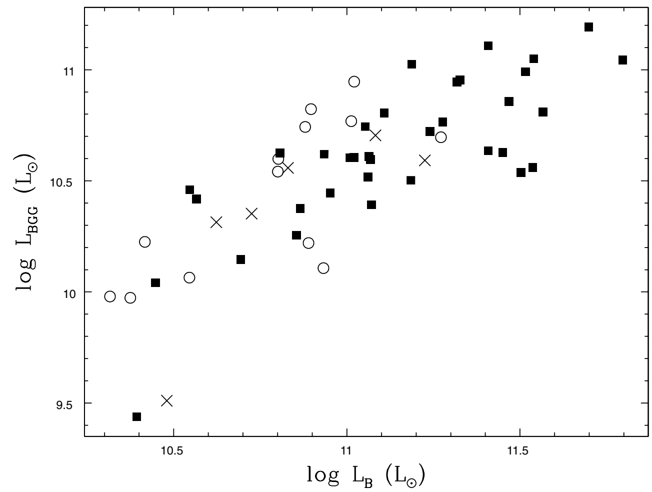

Figure 29. The relationship between $L_{\rm BGG}$ and $L_{\rm B}$. Filled squares represent the G-sample, open circles the H-sample and crosses non-detections.

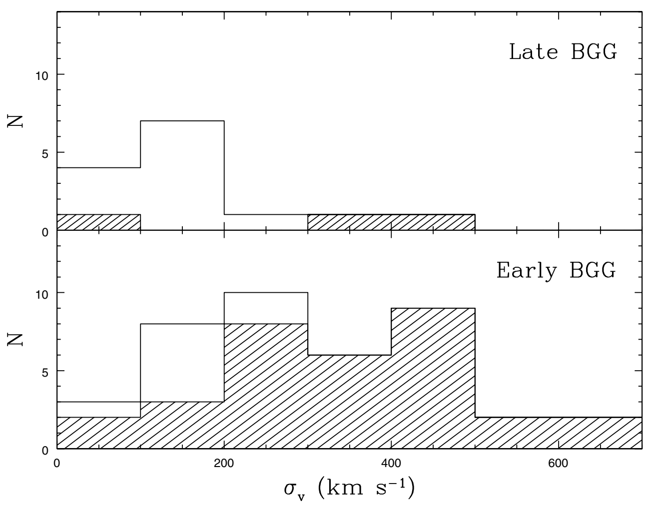

Figure 28. A histogram showing the distribution of $\sigma_{\rm v}$ for systems dominated by a late-type galaxy and those dominated by an early-type galaxy. The shaded region represents the G-sample.

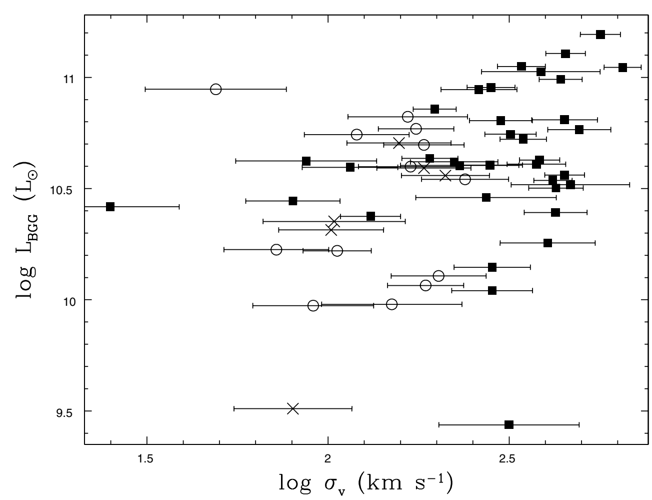

Figure 30. The relationship between $L_{\rm BGG}$ and $\sigma_{\rm v}$. Filled squares represent the G-sample, open circles the H-sample and crosses non-detections.

Finally we examine the issue of the dominance of the group BGGs and how this relates to other group properties. There is a class of groups, constituting ∼10 per cent of X-ray bright systems (Jones et al. 2003), in which the galaxy contents are dominated by a single luminous elliptical at least two magnitudes brighter than the second ranked galaxy. These have been dubbed fossil groups (Ponman et al. 1994), or overluminous elliptical galaxies (Vikhlinin et al. 1999). These are found to have unusually high ratios of X-ray to optical luminosity and are probably old groups in which the orbits of the major galaxies have had time to decay, leading to their merger into a central remnant (Jones et al. 2003). It has been suggested that the high L_X/L_B ratios may result from high gas density (and hence high L_X) resulting from an early formation epoch (Jones et al. 2003), or from an unusually low SFE, leading to low L_B (Vikhlinin et al. 1999). One might hope to derive some insights into the origin and properties of fossil groups from a study of the optical luminosity ratio between the first and second ranked galaxies (L_{12}) in the GEMS sample.

Only one of the GEMS systems qualifies as a fossil group, according to the definition of Jones et al. (2003), which requires $L_X > 10^{42} h_{50}^{-2}$ erg s^{-1}($h_{50} = H_0/50$) and $L_{12} > 6.3$ (2 mag). This system is NGC 741, which safely passes both thresholds. However, it displays neither the feature of high L_X/L_B, which is a feature of previously studied fossil groups, nor a high L_X for its temperature, which Jones et al. (2003) suggest may be another characteristic property of fossil systems. A study of the relationship between L_{12} and other statistical parameters, across the GEMS sample, reveals nothing very striking. For example, given the hypothesized link to merging, one might have expected to see a relationship with the spiral fraction or velocity dispersion of groups. However, neither of these shows any significant correlation (the relationship with f_{sp} is shown in Fig. 31), nor is there any very substantial difference between the distribution of L_{12} values for systems with early-type and late-type BGGs.

On the other hand, aparallel optical study of the luminosity function (Milesetal et al. 2004) has shown the presence of a distinctive dip in the luminosity function at $M_B \sim -18$ (which can be seen in Fig. 2), especially in low-L_X groups. A study of the structure of GEMS galaxies (Khosroshahi et al. 2004) provides further motivation for the suggestion that this dip might be generated by the effects of galaxy merging, which will generate brighter galaxies,

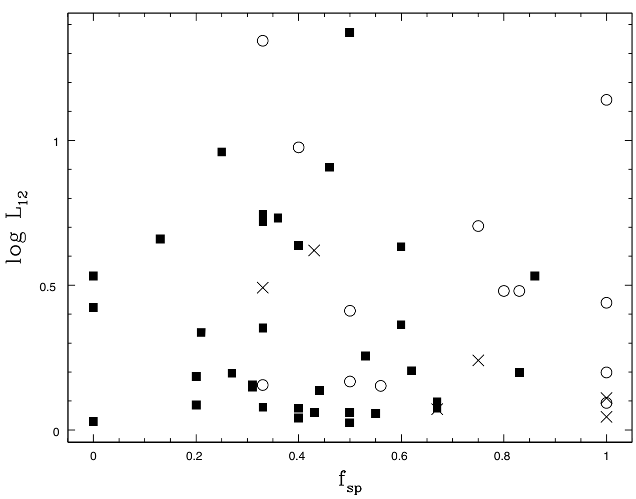

Figure 31. The relationship between L_{12} and f_{sp}. Filled squares represent the G-sample, open circles the H-sample and crosses non-detections.

whilst leaving the dwarfs relatively unaffected (as a result of their small merger cross-sections). If this is the case, then it appears that the opening up of a dip at intermediate magnitudes is not reflected strongly in the difference between first and second ranked galaxies, until the fossil stage is reached. This is understandable if merging affects all the brighter galaxies in a group, rather than simply the central BGG.

10 CONCLUDING DISCUSSION

Although the GEMS groups cannot be regarded as a proper statistically-selected sample, they do span a wider range in group properties than any previous sample subjected to a thorough X-ray analysis and statistical investigation. This has resulted in a number of new results and some challenges to findings from earlier work. Here we summarize and discuss some of the most important of these.

10.1 $L_X - T_X$

It has become widely accepted that the $L_X - T_X$ relation steepens in the group regime, following in part the results of Helsdon & Ponman (2000a), and much theoretical effort has been expended in trying to reproduce this steepening. It therefore comes as something of an embarrassment that the GEMS $L_X - T_X$ relation is consistent with an extrapolation of the $L_X \propto T_X^3$ trend seen in clusters. As we discussed in Section 7.1, this flatter $L_X - T_X$ slope cannot be regarded at present as a secure result, because a number of biases resulting from the large scatter in the properties of poor groups, coupled with the observational selection effect against detecting groups with very low L_X, conspire to systematically flatten the fitted relation. However, earlier results (e.g. Helsdon & Ponman 2000b) based on X-ray-selected group samples, showing a slope of 4–5, must now be regarded as questionable. The origin of the flatter relation found here appears to be primarily the inclusion of more groups with very low temperatures, some of which have surprisingly high X-ray luminosities.

Recent developments from studies of the entropy of groups and clusters tend to support the idea of a greater continuity in properties between the IGM in groups and clusters. The idea of a universal entropy floor (Ponman et al. 1999), which could have led to an isentropic IGM in the poorest systems (Babul et al. 2002) and hence to an $L_X - T_X$ slope of ∼5, has now been shown to be incorrect in two ways. First, individual groups do not show isentropic cores, as would be expected in such a simple pre-heating model (Mushotzky 2003; Ponman et al. 2003; Pratt & Arnaud 2003; Sun et al. 2003; Khosroshahi, Jones & Ponman 2004; Rasmussen & Ponman 2004) and secondly the scaling properties of entropy in clusters and groups appears to take the form of a ramp, rather than a floor (Ponman et al. 2003): following the non-self-similar power-law form $S \propto T_X^{0.65}$, rather than breaking from the self-similar slope of unity at a well-defined temperature $T_X \sim$ 1–2 keV, as was previously suggested (Lloyd-Davies, Ponman & Cannon 2000). Given this continuity of properties, a (non-self-similar) power-law form for the $L_X - T_X$ relation is what one would expect.

10.2 σ_v

We find several indications that the velocity dispersions of some poor groups are anomalously low. There are groups in our sample, such as HCG 16, HCG 22 and NGC 3665, which appear to have diffuse X-ray emission from a hot IGM [confirmed in the case of NGC 3665 and 1587 by the *Chandra* observations of Helsdon et al.

(2004)] and yet have velocity dispersions so low ($\lesssim$100 km s^{-1}) that it is hard to understand how they can be virialized. These groups also have very low values of $\beta_{\rm spec}(\lesssim 0.3)$, and if $\sigma_{\rm v}$ is used to calculate their overdensity radii, then the inferred values of galaxy density tend to be very high (Fig. 10). In Section 7.3, we discussed a number of statistical and physical effects that might lead to low values of $\sigma_{\rm v}$; however, statistical scatter cannot account for the lack of poor systems with high values of $\beta_{\rm spec}$ and statistical biases seem too weak to account for the very low values we observe. A more detailed investigation is required to determine whether alignment effects or tidal interactions can produce velocity dispersions as low as those observed.

10.3 Group radii

In order to make meaningful comparisons between the properties of groups and clusters, it is important to derive physical values within some well-defined overdensity radius. However, it has become apparent in the present study just how difficult it is to define a reliable value of r_{500} (r_{200} is even more difficult) in galaxy groups. Their low surface brightness prohibits the mapping of gas pressure (which would allow the mass to be inferred) out to large radii, even in X-ray bright groups. Virial analyses are unreliable as a result of the sparse galaxy populations and lensing studies are unfeasible on individual groups as a result of their low projected mass densities.

Having investigated the use of scaling formulae based on $\sigma_{\rm v}$, $T_{\rm X}$ and $L_{\rm B}$, we have reservations about all three. $\sigma_{\rm v}$ appears to be the worst of the three, as a result of the large unexplained biases in velocity dispersion in some poor groups, discussed above. $T_{\rm X}$ gives a much more stable and satisfactory estimate of group sizes, but there is some evidence that it may overestimate r_{500} by up to 40 per cent throughout the group regime. $L_{\rm B}$ also appears to give fairly stable results, but because there are both theoretical and observational reasons to believe that the mass-to-light ratio may drop in low-mass systems, a scaling formula based on constant SFE seems unwise. More work employing deep *XMM–Newton* observations to clarify the relationships between group masses and the value for $T_{\rm X}$ and $L_{\rm B}$ would be of great value for future scaling studies.

10.4 $\beta_{\rm fit}$

As was discussed in Section 8, it seems curious that the lower value of $\beta_{\rm fit}$ compared to clusters, which we believe to be a robust result, is not reflected in any significant correlation between $\beta_{\rm fit}$ and $T_{\rm X}$ within the GEMS sample. This appears to be another nail in the coffin of simple pre-heating models, which would lead to systematically flatter gas density profiles in the shallower potential wells of cool groups. We suggest that in our sample, such a weak trend may be obscured by fluctuations in the values of gas entropy between groups. This in turn may be driven by differences in the merger and star formation histories.

10.5 $f_{\rm sp}$

GEMS groups typically contain a much higher fraction of early-type galaxies than would be expected if one extrapolates the trends between $f_{\rm sp}$ and $T_{\rm X}$ or $L_{\rm X}$ established for clusters. This result is almost certainly related to the results of Helsdon & Ponman (2003b), who found that X-ray bright groups have lower $f_{\rm sp}$ than clusters, at a given projected density, and even at a given inferred three-dimensional density. They interpreted this result as evidence that galaxy morphology may be related to the effects of galaxy interactions and mergers, which are enhanced in low-velocity-dispersion systems.

It seems clear (Figs 27 and 28) that there is a class of groups with low $\sigma_{\rm v}$ and fairly high spiral fraction (including, in most cases, a late-type BGG) that show no group-scale X-ray emission. Because a hot, X-ray emitting IGM requires a collapsed group, both to heat the gas and to raise its density to the point where its emission becomes detectable, it seems very probable that these undetected groups are not yet virialized and represent late-forming groups. In a study of galaxy photometry for a subsample of 25 of the GEMS groups, Miles et al. (2004) find that groups with $L_{\rm X} < 5 \times 10^{41}$ erg s^{-1} (including some that are undetected) show a pronounced dip in their galaxy luminosity functions, which may result from the effects of recent galaxy merging activity taking place in these low-$\sigma_{\rm v}$ virializing systems.

10.6 BGGs

We confirm the very strong relationship between the presence of intergalactic X-ray emission and the presence of a centrally located luminous early-type galaxy, which has been noted by many previous authors. This points strongly to the effects of galaxy merging having played an important role during the evolution of these systems. However, we do find four groups from our G-sample, for which the early-type BGG does not lie at the centre of the X-ray emission and a further three systems in which the BGG is of late-type, as discussed in Section 9.2 above. The presence of a small fraction of systems in which the BGG is offset is not surprising, given that groups are expected to experience mergers during which their gravitational potentials will be perturbed. The three G-sample systems with late-type BGGs are all groups with compact cores. Two of them appear to be systems in the process of virialization, in which the gas has been recently heated, but a luminous early-type BGG has yet to form. The status of HCG 48 is still problematical and warrants more detailed study with better quality X-ray data.

Our richer groups tend to have more luminous BGGs (Figs 29 and 30), continuing a trend that has been noted in moderately rich clusters. Given the likelihood (Dubinski 1998) that these dominant early-type galaxies have been formed through multiple mergers, coupled with the strong inverse dependence of the merger cross-section on $\sigma_{\rm v}$ (Makino & Hut 1997), the positive correlation seen in Fig. 30 strongly suggests that much of this merging has taken place at earlier epochs, in substructures that have since merged to form the groups we observe today, because at the present epoch merging should be more effective in groups with low values of $\sigma_{\rm v}$.

ACKNOWLEDGMENTS

The authors would like to thank the other members of the GEMS project, especially Somak Raychaudhury, Duncan Forbes, Stephen Helsdon and Frazer Pearce, for their contributions to this work. The authors are also grateful to Alastair Sanderson and Don Horner for their help in making comparisons with cluster properties and to the referee for pointing out a number of areas where clarification was required. This research has made use of the LEDAS database at the University of Leicester, the NASA-IPAC Extragalactic Database and optical images from the STScI Digitised Sky Survey. The authors also acknowledge the support of a studentship (JPFO) and a Senior Fellowship (TJP) from the Particle Physics and Astronomy Research Council.

REFERENCES

Allen S. W., Fabian A. C., 1998, MNRAS, 297, 57
Allen S. W., Schmidt R. W., Fabian A. C., 2001, MNRAS, 328, L37
Arnaud M., Evrard A. E., 1999, MNRAS, 305, 631
Babul A., Balogh M. L., Lewis G. F., Poole G. B., 2002, MNRAS, 330, 329
Bahcall N. A., Comerford J. M., 2002, ApJ, 565, L5
Balogh M. L., Babul A., Patton D. R., 1999, MNRAS, 307, 463
Barton E., Geller M. J., Ramella M., Marzke R. O., da Costa L. N., 1996, AJ, 112, 871
Belsole E., Sauvageot J. L., Ponman T. J., Bourdin H., 2003, A&A, 398, 1
Benson A. J., Cole S., Frenk C. S., Baugh C. M., Lacey C. G., 2000, MNRAS, 311, 793
Bird C. M., Mushotzky R. F., Metzler C. A., 1995, ApJ, 453, 40
Blanton M. R. et al., 2003, ApJ, 592, 819
Böhringer H. et al., 2000, ApJS, 129, 435
Brough S., Collins C. A., Burke D. J., Mann R. G., Lynam P. D., 2002, MNRAS, 329, L53
Buote D. A., Fabian A. C., 1998, MNRAS, 296, 977
Burke D. J., Collins C. A., Mann R. G., 2000, ApJ, 532, L105
Cavaliere A., Menci N., Tozzi P., 1999, MNRAS, 308, 599
Dickey J. M., Lockman F. J., 1990, ARA&A, 28, 215
Dos Santos S., Mamon G. A., 1999, A&A, 352, 1
Dubinski J., 1998, ApJ, 502, 141
Ebeling H., Voges W., Boehringer H., 1994, ApJ, 436, 44
Edge A. C., 1991, MNRAS, 250, 103
Edge A. C., Stewart G. C., 1991a, MNRAS, 252, 414
Edge A. C., Stewart G. C., 1991b, MNRAS, 252, 428
Evrard A. E., Metzler C. A., Navarro J. F., 1996, ApJ, 469, 494
Feigelson E. D., Babu G. J., 1992, ApJ, 397, 55
Finoguenov A., Reiprich T. H., Böhringer H., 2001, A&A, 368, 749
Fouque P., Gourgoulhon E., Chamaraux P., Paturel G., 1992, A&AS, 93, 211
Frederic J. J., 1995, ApJS, 97, 259
Fukugita M., Shimasaku K., Ichikawa T., 1995, PASP, 107, 945
Garcia A. M., 1993, A&AS, 100, 47
Geller M. J., Huchra J. P., 1983, ApJS, 52, 61
Girardi M., Borgani S., Giuricin G., Mardirossian F., Mezzetti M., 1998, ApJ, 506, 45
Giudice G., 1999, in Giuricin G., Mezzetti M., Salucci P., eds, ASP Conf. Ser. Vol. 176, Observational Cosmology: The Development of Galaxy Systems. Astron. Soc. Pac., San Francisco, p. 136
Helsdon S. F., Ponman T. J., 2000a, MNRAS, 315, 356
Helsdon S. F., Ponman T. J., 2000b, MNRAS, 319, 933
Helsdon S. F., Ponman T. J., 2003a, MNRAS, 339, L29
Helsdon S. F., Ponman T. J., 2003b, MNRAS, 340, 485
Helsdon S. F., Ponman T. J., Mulchaey J. S., 2004, ApJ, submitted
Hickson P., 1982, ApJ, 255, 382
Hickson P., 1997, ARA&A, 35, 357
Hoekstra H. et al., 2001, ApJ, 548, L5
Horner D. J., 2001, PhD thesis, University of Maryland
Hradecky V., Jones C., Donnelly R. H., Djorgovski S. G., Gal R. R., Odewahn S. C., 2000, ApJ, 543, 521
Huchra J., Geller M., 1982, ApJ, 257, 423
Hwang U., Mushotzky R. F., Burns J. O., Fukazawa Y., White R. A., 1999, ApJ, 516, 604
Jones L. R., Ponman T. J., Horton A., Babul A., Ebeling H., Burke D. J., 2003, MNRAS, 343, 627
Kauffmann G., Charlot S., 1998, MNRAS, 294, 705
Khosroshahi H. G., Jones L. R., Ponman T. J., 2004, MNRAS, in press
Khosroshahi H. G., Raychaudhury S., Ponman T. J., Miles T. M., Forbes D. A., 2004, MNRAS, in press
Ledlow M. J., Loken C., Burns J. O., Hill J. M., White R. A., 1996, AJ, 112, 388
Lin Y., Mohr J. J., Stanford S. A., 2003, ApJ, 591, 749
Lloyd-Davies E. J., Ponman T. J., Cannon D. B., 2000, MNRAS, 315, 689
Mahdavi A., 2001, ApJ, 546, 812
Mahdavi A., Boehringer H., Geller M. J., Ramella M., 1997, ApJ, 483, 68
Mahdavi A., Böhringer H., Geller M. J., Ramella M., 2000, ApJ, 534, 114
Makino J., Hut P., 1997, ApJ, 481, 83
Mamon G. A., 1994, in Durret F., Mazure A., Tran Thanh Van J., eds, Clusters of Galaxies. Editions Frontières, Gif-sur-Yvette, p. 291
Markevitch M., 1998, ApJ, 504, 27
Matteucci F., Tornambe A., 1987, A&A, 185, 51
Mewe R., Lemen J. R., van den Oord G. H. J., 1986, A&AS, 65, 511
Miles T. A., Raychaudhury S. R., Forbes D. A., Goudfrooij P., 2004, MNRAS, submitted
Mohr J. J., Mathiesen B., Evrard A. E., 1999, ApJ, 517, 627
Muanwong O., Thomas P. A., Kay S. T., Pearce F. R., 2002, MNRAS, 336, 527
Mulchaey J. S., 2000, ARA&A, 38, 289
Mulchaey J. S., Zabludoff A. I., 1998, ApJ, 496, 73
Mulchaey J. S., Davis D. S., Mushotzky R. F., Burstein D., 1996, ApJ, 456, 80
Mulchaey J. S., Davis D. S., Mushotzky R. F., Burstein D., 2003, ApJS, 145, 39 (MDMB)
Mushotzky R., 2003, in Proc. IAU Symp. 216, X-ray Emission from Clusters of Galaxies. Kluwer, Dordrecht, p. 176
Navarro J. F., Frenk C. S., White S. D. M., 1995, MNRAS, 275, 720
Nevalainen J., Markevitch M., Forman W., 2000, ApJ, 532, 694
Nolthenius R., 1993, ApJS, 85, 1
O'Sullivan E. J., Ponman T. J., 2004, MNRAS, in press
O'Sullivan E. J., Ponman T. J., Collins R. S., 2003, MNRAS, 340, 1375
Pietsch W., Trinchieri G., Arp H., Sulentic J. W., 1997, A&A, 322, 89
Pildis R. A., Bregman J. N., Evrard A. E., 1995, ApJ, 443, 514
Ponman T. J., Allan D. J., Jones L. R., Merrifield M., McHardy I. M., Lehto H. J., Luppino G. A., 1994, Nat, 369, 462
Ponman T. J., Bourner P. D. J., Ebeling H., Böhringer H., 1996, MNRAS, 283, 690
Ponman T. J., Cannon D. B., Navarro J. F., 1999, Nat, 397, 135
Ponman T. J., Sanderson A. J. R., Finoguenov A., 2003, MNRAS, 343, 331
Pratt G. W., Arnaud M., 2003, A&A, 408, 1
Ramella M., Pisani A., Geller M. J., 1997, AJ, 113, 483
Rasmussen J., Ponman T. J., 2004, MNRAS, in press
Sanderson A. J. R., Ponman T. J., 2003, MNRAS, 345, 1241
Sanderson A. J. R., Ponman T. J., Finoguenov A., Lloyd-Davies E. J., Markevitch M., 2003, MNRAS, 340, 989
Sato S., Akimoto F., Furuzawa A., Tawara Y., Watanabe M., Kumai Y., 2000, ApJ, 537, L73
Sulentic J. W., Rosado M., Dultzin-Hacyan D., Verdes-Montenegro L., Trinchieri G., Xu C., Pietsch W., 2001, AJ, 122, 2993
Sun M., Forman W., Vikhlinin A., Hornstrup A., Jones C., Murray S. S., 2003, ApJ, 598, 250
Tully R. B., 1987, ApJ, 321, 280
Verde L. et al., 2002, MNRAS, 335, 432
Vikhlinin A., Forman W., Jones C., 1999, ApJ, 525, 47
White D. A., Jones C., Forman W., 1997, MNRAS, 292, 419
White R. A., Bliton M., Bhavsar S. P., Bornmann P., Burns J. O., Ledlow M. J., Loken C., 1999, ApJ, 118, 2014
Wu X., Xue Y., 2002, ApJ, 572, L19
Wu X., Xue Y., Fang L., 1999, ApJ, 524, 22
Xue Y., Wu X., 2000, ApJ, 538, 65
Zabludoff A. I., Mulchaey J. S., 1998, ApJ, 496, 39
Zabludoff A. I., Mulchaey J. S., 2000, ApJ, 539, 136

This paper has been typeset from a TEX/LATEX file prepared by the author.